

PEFT-Arena: Understanding Parameter-Efficient Finetuning from a Stability-Plasticity Perspective

Yangyi Huang^{1,†} Ruotian Peng^{2,†} Zeju Qiu³ Jiale Kang¹ Yandong Wen²
Bernhard Schölkopf³ Weiyang Liu^{1,3,*}

¹The Chinese University of Hong Kong ²Westlake University ³MPI for Intelligent Systems

[†]Equal contribution ^{*}Corresponding author SphereLab.ai/PEFT-Arena

Abstract

Parameter-efficient finetuning (PEFT) has become the standard approach for adapting large language models, yet evaluations largely emphasize downstream accuracy while overlooking the retention of pretrained capabilities. We argue that PEFT should be assessed through the stability-plasticity dilemma: the trade-off between target-task adaptation and resistance to forgetting. We introduce PEFT-Arena, a benchmark that jointly measures downstream performance and general capability retention. Across methods, we find distinct stability-plasticity profiles; under comparable parameter budgets, orthogonal finetuning achieves the most favorable Pareto frontier. To explain these differences, we analyze PEFT updates from two geometric perspectives. In weight space, spectral analysis reveals how parameterizations interact with the pretrained singular-value structure. In activation space, retention metrics show whether finetuning preserves or distorts general-capability representations, with forgetting linked to non-isometric representation distortion. Finally, an analysis shows that final SFT checkpoints often overshoot a better target-retention operating point. Inspired by this, we present case studies of a post-hoc improvement with path-wise rewinding.

1 Introduction

Parameter-efficient finetuning (PEFT) has become essential for adapting large foundation models to downstream tasks. By updating only a small subset of parameters, PEFT enables practical, low-cost deployment across diverse domains. But how should we determine whether a PEFT method is truly effective? Current practice often reduces this question to a single metric (*i.e.*, downstream task performance), while overlooking what the finetuned model may lose in the process. However, this single-metric paradigm can be misleading. A method that substantially improves mathematical reasoning while

silently degrading instruction following, factual recall, and general reasoning by a comparable margin has not truly adapted the model; rather, it has broken it. Although numerous PEFT methods have demonstrated strong effectiveness on downstream tasks, the extent to which they preserve pretrained capabilities after adaptation remains largely unclear. Therefore, the real question is not only “how much did the model learn?”, but also “how much did it learn relative to how much it forgot?” This is precisely characterized by the stability-plasticity dilemma (Mermillod et al., 2013): the tension between acquiring new capabilities (plasticity) and preserving existing ones (stability). Guided by this dilemma, we are interested in the question below:

Which PEFT method yields the most favorable stability-plasticity trade-off?

To this end, we introduce **PEFT-Arena**, a benchmark that jointly measures target-domain performance (plasticity) and general capability retention (stability) across two challenging reasoning domains, mathematics and medicine. With PEFT-Arena, we find that neither target performance nor general performance alone is sufficient for PEFT evaluation. All methods exhibit stability-plasticity trade-offs, but different parameterizations exhibit distinct trade-off patterns. In particular, orthogonal finetuning (OFT) often lies on a strong frontier, suggesting that the geometry of the update plays an important role in preserving general capabilities.

Benchmark results reveal the trade-offs induced by PEFT, but shed no light on how PEFT reshapes the model internally. It motivates another question:

Which internal mechanisms are associated with the stability-plasticity trade-off?

We approach this question from two complementary views. In *weight space*, we examine how PEFT updates interact with the pretrained spectral geome-

arXiv:2605.28819v1 [cs.LG] 27 May 2026

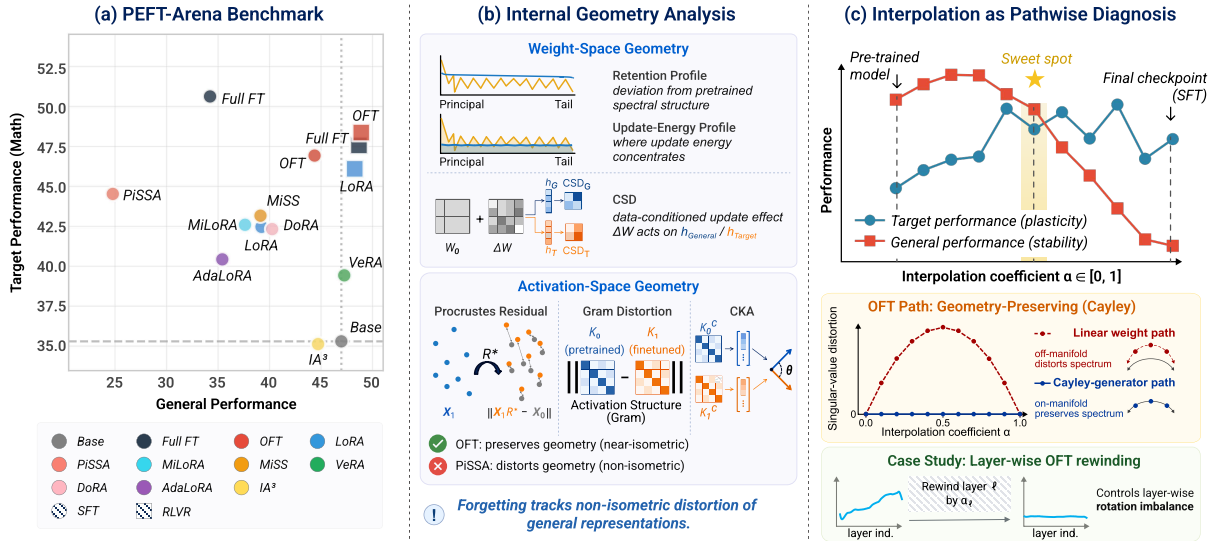


Figure 1: PEFT-Arena is designed to comprehensively evaluate the trade-off between downstream task adaptation and pretrained knowledge retention in LLM post-training with PEFT methods. (a) External stability–plasticity trade-offs across PEFT methods. (b) Internal geometry analysis from weight-space and activation-space views. (c) Interpolation reveals SFT overshoot and motivates pathwise rewinding along method-specific update paths.

try of weight matrices. This view highlights the inductive bias of each parameterization: additive low-rank methods, spectral-initialization variants, and orthogonal transformations reshape the pretrained basis in distinct ways. In *activation space*, we examine the representations induced by the finetuned model on the same evaluation examples. The key issue is not simply whether activations move, but whether finetuning preserves the relative structure among examples that the pretrained model represented coherently. We measure this non-isometric distortion using Procrustes residual, pairwise Gram distortion, and linear CKA. This view links forgetting to representation-geometry damage. We find that OFT better preserves the structure of general representation than other PEFT methods.

Finally, we use interpolation as a pathwise diagnostic of finetuning dynamics:

Can interpolation reveal where PEFT loses stability along the adaptation path?

Weight interpolation between the base and finetuned model exposes a common SFT overshoot phenomenon, *i.e.*, the final checkpoint often moves beyond the best target-retention operating point. We use interpolation as a diagnostic tool to study the stability-plasticity trade-off. Moreover, interpolation must respect each PEFT method’s natural update geometry. For additive methods, the natural path scales the additive update ΔW ; for

OFT, the natural path scales the skew-symmetric Cayley generator rather than linearly interpolating dense weights. Within this view, layer-wise OFT rewinding serves as a practical example of post-hoc control for imbalanced update strength. Our contributions are listed below:

- **A multi-faceted PEFT benchmark.** We evaluate PEFT methods based on both target-domain gains and general capability preservation.
- **Findings on PEFT trade-off patterns.** We show that PEFT methods exhibit distinct stability-plasticity behavior, and that OFT often provides a strong frontier under the same parameter budget.
- **Internal analysis from weight and activation geometry.** We connect external forgetting to internal changes through two empirical views: spectral profiles of weight updates and non-isometric distortion of activation geometry.
- **Interpolation as pathwise diagnosis.** We use interpolation to diagnose SFT overshoot and emphasize parameterization-aware interpolation paths, with OFT’s Cayley path and layer-wise rewinding illustrating geometry-aware control.

2 The PEFT-Arena Benchmark

2.1 Experimental Setup

All PEFT methods are evaluated along two axes: (i) target-domain performance and (ii) general ability retention. We use target-domain performance as a

proxy for *plasticity*, and general-task performance as a proxy for *stability*. We conduct experiments on two target domains, mathematics and medicine, under two post-training settings: supervised finetuning (SFT) and reinforcement learning with verifiable rewards (RLVR). Unless otherwise stated, we report average accuracy (%) for each domain.

Target-domain benchmarks and evaluation.

(i) *Math*: We evaluate on a combined set of Math-500 (Lightman et al., 2023), AMC23, and AIME24.

(ii) *Medicine*: We evaluate on a collection of medical reasoning and knowledge benchmarks, including MedMCQA (Pal et al., 2022), MedQA (USMLE) (Jin et al., 2021), PubMedQA (Jin et al., 2019), MMLU-Pro (Wang et al., 2024b), GPQA (Medical) (Rein et al., 2024), Lancet, NEJM & MedBullets problems (Chen et al., 2025), and MedXpertQA (Zuo et al., 2025) following a dedicate dataset survey (Huang et al., 2025).

General ability retention. To measure general ability preservation after adaptation, we evaluate on IFEval (Zhou et al., 2023), NQ (Kwiatkowski et al., 2019), BBH (Suzgun et al., 2023), covering instruction following, natural language understanding, general knowledge and general reasoning. We use the average score (%) across these tasks as our General score to assess model forgetting after finetuning. We follow an OpenCompass-style evaluation configuration with context length 1024, temperature $T = 0.0$, and one sample per query.

Base models and adaptation methods. We use Qwen2.5-7B (Yang et al., 2024) and Llama3.2-3B-Instruct (Dubey et al., 2024) as pretrained LLMs to cover different scales and base/instruction-tuned settings. We compare full finetuning (Full FT) against a representative set of PEFT baselines (see Appendix A for related work details). (i) *Additive PEFT (LoRA family)*: We include LoRA (Hu et al., 2022) and representative variants spanning rank allocation, parameterization and initialization: AdaLoRA (Zhang et al., 2023), DoRA (Liu et al., 2024a), MiSS (Kang and Yin, 2026), VeRA (Kopiczko et al., 2024), PiSSA (Meng et al., 2024), and MiLoRA (Wang et al., 2025). We also include KeepLoRA (Luo et al., 2026), an anti-forgetting LoRA variant that constrains updates away from the principal subspace. (ii) *Multiplicative PEFT*: We include orthogonal finetuning (OFT) (Qiu et al., 2023; Liu et al., 2024b; Qiu et al., 2025), which constrains updates to structured orthogonal transformations with adjustable sparsity. (iii) *Activation-based PEFT*: We include IA³ (Liu

et al., 2022a), a lightweight method that adapts models via learned activation scaling.

To fairly compare PEFT method under a similar parameter budget, Table 1 includes budget-matched SFT slices rather than a single configuration per method. On Qwen, the roughly 20M trainable-parameter group compares OFT-b32 (17.55M) with LoRA/PiSSA/MiLoRA/KeepLoRA-r8 (20.19M) and DoRA-r8 (21.58M), while the roughly 40M group compares OFT-b64 (35.68M) with LoRA-r16 (40.37M), with the Llama columns reporting the corresponding backbone-specific counts.

Training and optimization details. We conduct SFT in both target domains, using 50k filtered samples from OpenR1-Math-330k (Hugging Face, 2025) for math and 23k samples from m23k (Huang et al., 2025) for medical. We also include RLVR results with GRPO (Shao et al., 2024) on a representative subset of methods for comparison. Full details are provided in Appendix B.

2.2 Main Results and Discussions

We report benchmark results along two axes: target-domain performance (plasticity) and general ability retention (stability), under both SFT and RLVR settings. The complete results are given in Table 1. In the following, we summarize the key empirical findings. Unless otherwise specified, all changes relative to the corresponding base model are absolute differences in percentage points.

SFT improves target performance at the expense of general ability. In Table 1, Full FT gives the largest target gains but it also incurs the most severe forgetting. On Qwen2.5-7B, Full FT increases the math target accuracy from 35.30 to 50.63 and the medical target accuracy from 46.36 to 53.63, while the general performance drops from 46.97 to 34.22 for math and drops from 46.97 to 34.41 for medicine. On Llama3.2-3B-Instruct, the general performance falls from 53.03 to 26.03 for medicine. The results suggest that target-only reporting systematically overestimates post-training quality.

Under SFT, methods show distinct trade-off patterns, with OFT on the best frontier. Within the additive low-rank family, LoRA, MiSS, DoRA, and AdaLoRA generally improve target performance but tend to incur non-trivial forgetting, with larger adaptation capacity usually pushing further toward plasticity. For example, on Qwen math, LoRA-r8 improves target by 7.17 with a 7.75 general drop, while MiSS-r64 reaches 11.63 target gain with a 14.20 general drop. SVD-guided variants

Method	Settings	Tr. Param (Qwen)	Qwen2.5-7B-base				Tr. Param (Llama)	Llama3.2-3B-Instruct			
			Math Target (%)	Math General (%)	Med Target (%)	Med General (%)		Math Target (%)	Math General (%)	Med Target (%)	Med General (%)
<i>Supervised FineTuning (SFT)</i>											
Base	-	7.61B	35.30 (+0.00)	46.97 (+0.00)	46.36 (+0.00)	46.97 (+0.00)	3.21B	27.80 (+0.00)	53.03 (+0.00)	41.44 (+0.00)	53.03 (+0.00)
Full FT	-	7.61B	50.63 (+15.33)	34.22 (-12.74)	53.63 (+7.27)	34.41 (-12.56)	3.21B	33.90 (+6.27)	39.83 (-13.20)	44.26 (+2.82)	26.03 (-27.00)
OFT	block 16	8.49M	42.33 (+7.03)	42.58 (-4.39)	46.17 (-0.19)	45.09 (-1.88)	7.08M	29.43 (+1.80)	41.08 (-11.95)	39.22 (-2.22)	40.97 (-12.06)
OFT	block 32	17.55M	46.93 (+11.63)	44.37 (-2.60)	48.63 (+2.27)	42.40 (-4.57)	11.55M	30.60 (+2.97)	40.73 (-12.30)	39.50 (-1.94)	40.50 (-12.53)
OFT	block 64	35.68M	46.23 (+10.93)	35.97 (-11.00)	49.47 (+3.11)	39.11 (-7.86)	24.97M	29.30 (+1.67)	39.75 (-13.28)	40.77 (-0.67)	37.70 (-15.33)
OFT	block 128	71.92M	47.77 (+12.47)	36.98 (-9.99)	52.40 (+6.04)	36.88 (-10.08)	47.34M	32.23 (+4.60)	36.26 (-16.76)	42.17 (+0.73)	34.26 (-18.77)
LoRA	r4a8	10.09M	42.33 (+7.03)	41.66 (-5.31)	47.12 (+0.76)	36.42 (-10.55)	6.9M	24.30 (-3.33)	35.79 (-17.23)	36.92 (-4.52)	31.84 (-21.19)
LoRA	r8a16	20.19M	42.47 (+7.17)	39.22 (-7.75)	47.91 (+1.55)	36.06 (-10.91)	12.16M	24.07 (-3.56)	36.57 (-16.46)	38.34 (-3.10)	27.99 (-25.04)
LoRA	r16a32	40.37M	44.87 (+9.57)	34.91 (-12.06)	47.86 (+1.51)	34.86 (-12.11)	24.31M	24.97 (-2.66)	37.55 (-15.48)	39.21 (-2.23)	29.18 (-23.85)
LoRA	r32a64	80.74M	45.37 (+10.07)	38.21 (-8.76)	49.48 (+3.12)	35.50 (-11.47)	48.63M	25.90 (-1.73)	37.20 (-15.83)	39.33 (-2.11)	30.69 (-22.34)
AdaLoRA	r8a16	30.28M	40.43 (+5.13)	35.41 (-11.56)	45.22 (-1.13)	37.34 (-9.63)	18.24M	20.83 (-6.80)	34.53 (-18.49)	37.11 (-4.33)	36.29 (-16.74)
PiSSA	r8a16	20.19M	44.53 (+9.23)	24.78 (-22.19)	26.16 (-20.19)	18.05 (-28.92)	12.16M	0.67 (-26.96)	9.74 (-43.28)	21.17 (-20.27)	12.92 (-40.11)
MiLoRA	r8a16	20.19M	42.60 (+7.30)	37.62 (-9.35)	46.83 (+0.48)	35.88 (-11.09)	12.16M	23.60 (-4.03)	35.59 (-17.44)	37.64 (-3.81)	29.23 (-23.80)
KeepLoRA	r8	20.19M	40.53 (+5.23)	43.75 (-3.22)	45.60 (-0.76)	47.09 (+0.12)	12.16M	15.20 (-12.43)	40.74 (-12.29)	41.26 (-0.18)	39.52 (-13.51)
MISS	r8	11.12M	43.17 (+7.87)	39.12 (-7.85)	48.75 (+2.40)	34.43 (-12.54)	6.19M	23.37 (-4.26)	33.93 (-19.09)	40.16 (-1.28)	31.71 (-21.32)
MISS	r64	89.00M	46.93 (+11.63)	32.77 (-14.20)	51.90 (+5.54)	32.72 (-14.25)	49.55M	28.63 (+1.00)	34.96 (-18.06)	41.96 (+0.52)	22.78 (-30.25)
VeRA	r256	1.44M	39.43 (+4.13)	47.25 (+0.38)	28.50 (-17.85)	47.01 (+0.04)	0.82M	28.80 (+1.17)	46.79 (-6.23)	40.68 (-0.76)	48.94 (-4.09)
DoRA	r8a16	21.58M	42.33 (+7.03)	40.25 (-6.72)	48.04 (+1.69)	36.06 (-10.91)	12.93M	23.83 (-3.80)	35.65 (-17.37)	38.25 (-3.19)	27.53 (-25.50)
IA ³	-	1.82M	35.13 (-0.17)	44.71 (-2.26)	30.08 (-16.28)	48.25 (+1.28)	0.92M	29.70 (+2.07)	45.72 (-7.30)	39.13 (-2.31)	45.67 (-7.36)
<i>RLVR with Group Relative Policy Optimization (GRPO)</i>											
Full FT	-	7.61B	47.57 (+12.27)	48.68 (+1.71)	46.24 (-0.11)	43.22 (-3.75)	3.21B	29.80 (+2.17)	52.20 (-0.82)	45.88 (+4.44)	51.81 (-0.83)
OFT	block 32	17.55M	47.90 (+12.60)	48.90 (+1.93)	46.79 (+0.44)	47.24 (+0.27)	11.55M	29.97 (+2.34)	50.04 (-2.98)	44.99 (+3.55)	52.31 (-2.99)
LoRA	r8a16	20.19M	46.93 (+11.63)	48.27 (+1.30)	47.08 (+0.73)	42.80 (-4.17)	12.16M	28.83 (+1.20)	52.17 (-0.85)	44.97 (+3.53)	53.53 (-0.86)

Table 1: Main benchmark results. For each domain, average task accuracy is reported in % (higher is better). We also report the absolute change relative to the corresponding base model in parentheses. Trainable-parameter columns show the comparable parameter budget for different methods.

(MiLoRA and especially PiSSA), which rely on initialization or subspace selection, are less stable in this benchmark: PiSSA-r8 improves Qwen math target by 9.23 but drops Qwen math general by 22.19 and Qwen medical target by 20.19. The anti-forgetting LoRA variant, KeepLoRA, partially improves knowledge retention: on Qwen it raises math general from 39.22 (LoRA-r8) to 43.75 and even preserves medical general ability at 47.09, but its target adaptation is much weaker and it does not dominate the frontier across settings, especially on Llama. This suggests that retention-oriented subspace constraints alone do not guarantee the strongest overall trade-off. Outside LoRA-style methods, IA³ (activation scaling) and VeRA (shared frozen projection matrices with a small number of trainable scaling vectors) are both highly parameter-efficient and relatively conservative: VeRA preserves Qwen general ability best (math/medical general: +0.38/+0.04) but sacrifices medical target performance (-17.85), while IA³ shows a similar low-plasticity profile. In contrast, OFT’s spectrum-preserving multiplicative parameterization gives the best balance between adaptation and retention: OFT-b32 improves Qwen math target by 11.63 with only a 2.60 drop on math general, forming the strongest stability-plasticity frontier among PEFT baselines. This frontier is not only a comparison across methods but also across comparable trainable-parameter budgets: in the roughly 20M Qwen group, OFT-b32 is compared against

LoRA/PiSSA/MiLoRA/KeepLoRA-r8 and DoRA-r8, and in the roughly 40M group, OFT-b64 is compared against LoRA-r16.

RLVR generally enables stable adaptation while causing less forgetting. Compared with SFT, RLVR with GRPO exhibits a qualitatively different regime. On Qwen math adaptation, Full FT, OFT, and LoRA improve target by 12.27, 12.60, and 11.63, while their math-general scores also increase by 1.71, 1.93, and 1.30. OFT remains slightly above Full FT on target performance (47.90 vs. 47.57) with far fewer trainable parameters (17.55M vs. 7.61B), while LoRA reaches 46.93 with 20.19M trainable parameters. This behavior is consistent with on-policy optimization, where updates are anchored to the model’s own trajectories; under this regime, structured PEFT parameterizations can better capture the RL objective efficiently without large functional drift.

Longer GRPO training reveals a related high- k degradation pattern. From Table 2, we observe that longer GRPO training reveals a related pathwise degradation pattern under high- k evaluation. Pass@1 target performance remains relatively stable, but high- k sampling can degrade after extended optimization, with Full FT and LoRA showing larger pass@64 drops than OFT. This resembles SFT over-adaptation from a different evaluation angle. We revisit this pathwise view in section 4, where interpolation diagnoses SFT overshoot; Appendix F.6 further suggests that in-

terpolation can also partially recover longer-RLVR high- k degradation. Beyond the main General axis, Appendix C.1 reports expanded validation on HumanEval, HellaSwag, WinoGrande, MMLU(avg), ARC, and GSM8K. These additional benchmarks are consistent with the General axis in Table 1 and broaden our coverage of general capabilities.

Takeaway. *In SFT, PEFT method exhibits drastically different stability-plasticity trade-offs. SFT is less resistant to forgetting than RLVR. Among all methods, OFT often lies on the favorable frontier, highlighting the value of spectrum preservation.*

The benchmark shows *what* trade-offs occur, but it does not explain *how* different PEFT parameterizations change the model internally. Next, we propose to analyze PEFT updates through weight-space and activation-space geometry, with a focus on how these changes affect general capabilities.

3 Understanding PEFT Updates through Internal Geometry

PEFT-Arena exposes external stability-plasticity trade-offs, but benchmark scores alone do not explain how different parameterizations preserve or disrupt general capabilities. We therefore analyze PEFT updates from two complementary internal views. The *weight-space* view examines how updates interact with the spectral geometry of pretrained parameters. The *activation-space* view measures how much finetuning distorts the pairwise structural similarity of representations induced by general-evaluation data, which provides a direct view of capability retention.

3.1 Weight-Space Geometry

Inspired by prior work (Biderman et al., 2024; Zhu et al., 2025; Mukherjee et al., 2025; Martin and Mahoney, 2021), we start by analyzing PEFT updates in the pretrained spectral basis. We use two descriptive measures of weight-space geometry: a *retention* profile, which measures how much the pretrained singular structure is preserved, and an *adaptation* profile, which measures where update energy is injected. These profiles characterize the update geometry induced by different PEFT parameterizations; in the next subsection, we complement them with activation-space diagnostics that measure whether the resulting representations preserve the structure of general-evaluation data.

Let the pretrained weight be decomposed as

$W_0 = U\Sigma V^\top$, where u_i and v_i are the i -th left and right singular vectors. We study a finetuned weight W^* from two complementary views.

Retention profile: diagonal projection on the pretrained basis. We measure how much W^* preserves the pretrained singular alignment via

$$\begin{aligned} P_{\text{diag}}(i) &= u_i^\top W^* v_i, \\ |\Delta P_{\text{diag}}(i)| &= \left| u_i^\top (W^* - W_0) v_i \right|. \end{aligned} \quad (1)$$

The quantity $|\Delta P_{\text{diag}}(i)|$ measures component-wise deviation from the pretrained singular structure. Large or irregular changes indicate stronger perturbation of principal directions that may support pretrained general capabilities.

Adaptation profile: update energy over pretrained directions. To capture where the update injects energy, we project the effective update $\Delta W = W^* - W_0$ onto pretrained input directions:

$$E_\Delta(i) = \|\Delta W v_i\|_2. \quad (2)$$

Compared with the diagonal projection, $E_\Delta(i)$ captures both scaling changes and off-diagonal rotations along the i -th latent direction. We use this profile as a description of how different PEFT parameterizations allocate update energy, not as a standalone explanation of target-domain gains.

Descriptive spectral smoothness. Figure 2 visualizes the retention and update-energy profiles. We summarize local irregularity with a fluctuation score, defined in Appendix D.1, and use it only as a descriptive measure rather than a formal taxonomy. The main pattern is that PiSSA and MiSS show large retention-side deviations, LoRA exhibits spiky update-energy allocation, and OFT maintains a more structured retention profile under its orthogonal parameterization. Full spectral profiles and smoothness statistics are provided in Appendix D.1; additional OFT-specific singular-vector diagnostics are provided in Appendix D.2.

Capability-conditioned drift. The spectral profiles describe where an update acts, but not whether those directions are used by a data distribution. We therefore compute the following quantity:

$$\text{CSD}_D = \mathbb{E}_{x \sim D} \frac{\|\Delta W h_0(x)\|_2^2}{\|W_0 h_0(x)\|_2^2 + \epsilon}. \quad (3)$$

where $h_0(x)$ is the pretrained activation. Intuitively, CSD_D weights update energy by how strongly dataset D activates the corresponding directions. We find that CSD_G is associated with forgetting,

Method	AIME24		AMC23		MATH500		AVG	
	pass@1	pass@64	pass@1	pass@64	pass@1	pass@64	pass@1	pass@64
Full FT	13.9 / 15.1	50.0 / 40.0	52.7 / 55.1	92.5 / 87.5	76.1 / 76.6	93.2 / 93.4	47.57 / 48.93	78.57 / 73.63
LoRA	11.4 / 14.8	43.3 / 36.7	54.6 / 57.4	92.5 / 92.5	74.8 / 75.5	94.4 / 92.2	46.93 / 49.23	76.73 / 73.80
OFT	16.5 / 15.4	46.7 / 43.3	52.8 / 51.9	90.0 / 90.0	74.4 / 76.2	95.0 / 94.0	47.90 / 47.83	77.23 / 75.77

Table 2: Longer-RLVR high- k evaluation. Each entry denotes the result at Step 200 (left) and Step 500 (right).

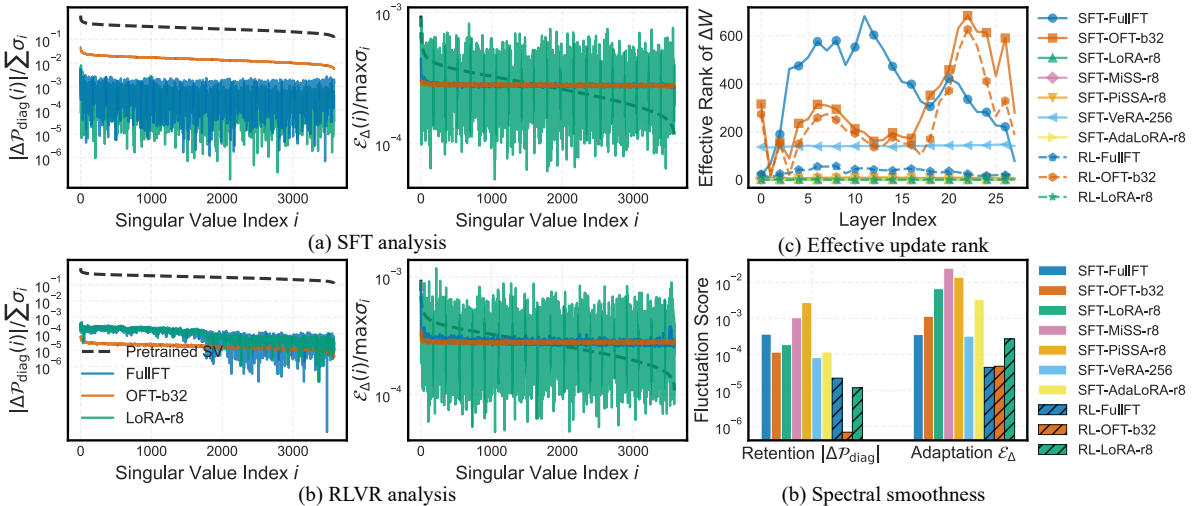


Figure 2: Weight-space spectral retention-adaptation profiling. (a & b) Distributions of projected spectrum changes (retention and adaptation profiles). (c) Effective rank of weight updates on all down_proj layers. (d) Fluctuation scores that quantify spectral smoothness of retention and adaptation profiles.

while CSD_T is not a simple predictor of target gain. Since CSD measures raw displacement and does not distinguish rotation-like movement from non-isometric distortion, we use it as a bridge from weight profiles to the activation-geometry analysis below, and full results are in Appendix D.3.

3.2 Activation-Space Geometry

Weight-space geometry does not directly tell us whether an update damages concrete capabilities. We therefore compare base-model activations and finetuned-model activations on the same general examples for Qwen2.5-7B and Llama3.2-3B-Instruct checkpoints from the main table. We collect full-forward module outputs on general data (IFEval, NQ, BBH); the tested layer/module locations and full breakdown are reported in Appendix E.

We use three complementary diagnostics. First, Procrustes residual removes the best shared orthogonal alignment between centered base activations X_0 and finetuned activations X_1 :

$$d_{\text{proc}} = \frac{\min_{R^T R=I} \|X_1 R - X_0\|_F}{\|X_0\|_F + \epsilon}. \quad (4)$$

A large residual indicates non-isometric distortion beyond a benign rotation. Second, linear CKA (Kornblith et al., 2019) measures representation sim-

Metric	External metric	Pearson	Spearman
Procrustes residual	Forgetting	0.711	0.568
Gram distortion	Forgetting	0.485	0.361
CKA	Forgetting	-0.761	-0.711

Table 3: Activation-geometry correlations between general-data representation geometry and forgetting across 20 SFT checkpoints of representative methods and eight module locations. Procrustes residual and Gram distortion measure non-isometric distortion, while CKA measures representation similarity.

ilarity through centered Gram matrices. Third, pairwise Gram distortion compares the cosine-similarity structure among examples and is insensitive to a shared orthogonal rotation. Full definitions and detailed metrics are given in Appendix E.1.

Table 3 summarizes the main correlations over general-distribution activation rows. Procrustes residual on general data strongly correlates with forgetting. Linear CKA shows the complementary trend, while pairwise Gram distortion also supports the relational-geometry interpretation with a weaker correlation.

Table 4 compares the activation geometry patterns across different PEFT methods. OFT exhibits lower non-isometric distortion and higher CKA than LoRA and full fine-tuning, whereas PiSSA emerges as a clear outlier, showing the strongest

Method	Proc. ↓	Gram ↓	CKA ↑	Forget ↓
Full FT	0.1640	0.2500	0.8654	17.31
LoRA	0.1808	0.2430	0.8564	15.97
OFT	0.1279	0.1906	0.9340	7.81
MiLoRA	0.1635	0.2476	0.8651	16.35
PiSSA	0.4376	0.8655	0.4402	34.56

Table 4: Activation-geometry on general data for one representative module slice over SFT checkpoints. We average the results for each method, and the complete layer/module breakdown is in Appendix E.3. Procrustes residual and Gram distortion measure non-isometric distortion, while CKA measures representation similarity.

distortion and the most severe forgetting. This suggests that OFT’s advantage in general-capability retention is reflected not only in the geometry of the weights, but also in the functional geometry of the representations that support general capabilities.

These metrics are used as retention-side diagnostics. We do not use them to explain target-task gains, since plasticity on reasoning-heavy math and medical tasks may depend on task-aligned computation, answer margins, and multi-step reasoning behavior beyond representation geometry.

Taken together, these two internal perspectives clarify why retention varies across PEFT methods. Weight-space profiles characterize the update bias induced by each parameterization, while activation-space diagnostics indicate whether the resulting representations used for general evaluation remain geometrically stable. OFT better preserves this geometry, whereas PiSSA substantially distorts it.

Takeaway. PEFT’s general-capability retention is strongly associated with preserving the representation geometry of general-evaluation data.

4 Interpolation as a Pathwise Study

The analyses above compare the base and final finetuned models, but the final checkpoint represents only a single point along the adaptation trajectory. A method may acquire most of its target-domain gains before reaching this endpoint, while continued movement along the trajectory can further erode general capabilities. This motivates a pathwise question: has the final checkpoint moved farther than necessary to achieve its target-task gains? We use interpolation to probe this question. Rather than treating interpolation as a new evaluation protocol or adaptation technique, we use it as a diagnostic tool to trace how target performance and general retention change as the model moves from the base checkpoint toward the adapted checkpoint.

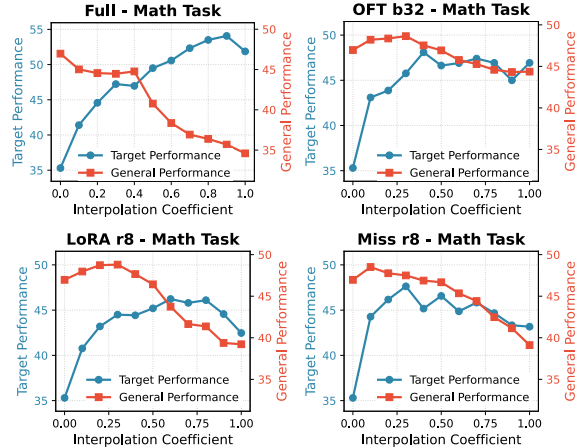


Figure 3: Target-general performance trade-off with α -interpolation for PEFT methods. Interpolation is used as a pathwise diagnostic of SFT overshoot. Additive methods are interpolated by scaling ΔW ; OFT is interpreted through its parameterization-aware Cayley path.

4.1 Finetuning Overshoots the Best Trade-off

For full finetuning and additive PEFT methods, the natural path scales the effective update ΔW . Sweeping this coefficient exposes a target-retention curve. In SFT, we consistently observe that the final checkpoint lies past a better operating point, and reducing the update strength can recover general ability while preserving much of the target gain.

Let W_0 be the pretrained weight and W^* be the finetuned effective weight. For full finetuning and additive PEFT methods, the natural interpolation is

$$W(\alpha) = W_0 + \alpha(W^* - W_0), \quad \alpha \in [0, 1], \quad (5)$$

where $\alpha = 0$ recovers the base model and $\alpha = 1$ recovers the final adapted model. Sweeping α exposes a pathwise stability-plasticity curve.

Figure 3 shows that SFT checkpoints often exhibit an overshoot phenomenon: the final checkpoint is not always the best target-retention operating point. Moving back along the interpolation path can recover general ability while preserving much of the target gain. This is not meant to replace final-checkpoint evaluation; instead, it diagnoses where stability is lost along the adaptation path.

Figure 4 further compares the actual training trajectory with the interpolation trajectory. The two paths exhibit totally different patterns, with the training trajectory being concave and the interpolation trajectory being convex. This distinction suggests that the SFT overshoot phenomenon is not merely a consequence of late-stage overfitting, and that the optimal stability-plasticity trade-off cannot be attained through early stopping. We have

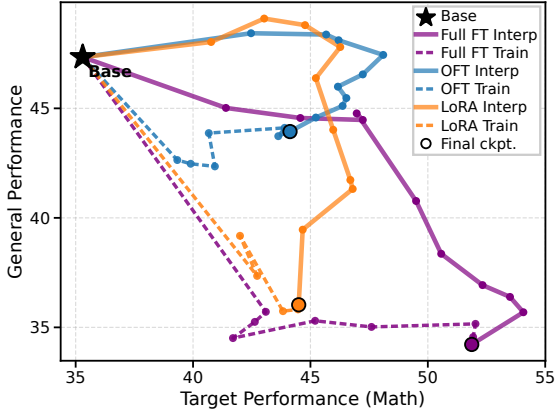


Figure 4: Training trajectory versus interpolation trajectory in the target-general plane. Dotted curves follow saved optimization checkpoints, while solid curves sweep α along the interpolation path between the base model and the final checkpoint.

also discussed a similar overshoot pattern of longer-horizon RLVR high- k degradation in Appendix F.6.

4.2 Parameterization-Aware Interpolation

Different PEFT parameterizations have different natural interpolation coordinates. For additive methods, scaling ΔW gives the natural path. For OFT, adaptation is parameterized by a skew-symmetric generator Q and an orthogonal Cayley transform, so dense-weight interpolation leaves the OFT manifold. We therefore interpolate by scaling the generator, $R(\alpha) = \text{Cayley}(\sqrt{\alpha}Q)$, where α controls rotation strength. This path preserves the intended orthogonal geometry; dense-weight interpolation is used only as a diagnostic baseline.

We empirically find that this distinction matters. On Qwen2.5-7B SFT-math with OFT-b32, the $\sqrt{\alpha}Q$ path gives a better target-retention frontier than dense-weight delta interpolation: at $\alpha = 0.3$, it reaches 45.77 math and 48.64 General, while the linear interpolation (as in Equation 5) at the same α gives 43.93 math and 43.91 General. Implementation details and the complete interpolation comparison are reported in Appendix F.1, F.3.

4.3 Layer-wise Interpolation for OFT

The parameterization-aware view also prompts us to reconsider whether a single global interpolation coefficient is too coarse. We observe that OFT updates are imbalanced across depth, with later layers often receiving substantially larger rotation strengths than early layers (see the evidence in Figure 8 of Appendix F.4); uniform interpolation rewinds all layers using the same coefficient and therefore cannot correct this layer-wise imbalance.

Variant	Target (Math)	General (Math)	Target (Med)	General (Med)
Finetuned	46.93 (+11.63)	44.37 (-2.60)	48.63 (+2.27)	42.40 (-4.57)
Uniform scal. 0.8	46.93 (+11.63)	44.82 (-2.15)	49.17 (+2.81)	45.76 (-1.21)
Uniform scal. 0.4	48.10 (+12.80)	47.53 (+0.56)	48.83 (+2.47)	48.15 (+1.18)
Layer. scal. (Safe)	47.17 (+11.87)	46.69 (-0.28)	50.01 (+3.65)	47.61 (+0.64)
Layer. scal. (Min)	47.83 (+12.53)	46.86 (-0.11)	49.76 (+3.41)	47.79 (+0.82)

Table 5: OFT post-hoc rewinding case study. Layer-wise generator scaling can recover general ability while preserving much of the target gain.

To further investigate this, we perform a simple layer-wise rewinding experiment. Instead of applying one coefficient to all layers, we rescale each layer’s generator Q_ℓ separately while staying on the OFT manifold. **SafeScale** uses the empirical average update strength of the first five layers (for Qwen2.5-7B) as the reference and scales other layers toward it, while **MinScale** uses the weakest-updated layer as the reference. As shown in Table 5, layer-wise rewinding improves the target-retention trade-off relative to the final OFT checkpoint. These results suggest that SFT overshoot is not only related to the total update magnitude, but also to how adaptation strength is allocated across layers. The improvement from this sweeping-free adjustment indicates that adaptively choosing rewinding strengths for different layers is a promising direction for post-hoc trade-off control. Additional results for OFT and LoRA/MiSS variants are reported in Appendix F.4, F.5.

5 Concluding Remarks

We introduce PEFT-Arena to evaluate PEFT methods through the stability-plasticity trade-off rather than target accuracy alone. Parameterizations differ substantially in how they exchange target gains for general-capability retention, with OFT often defining a strong frontier at comparable parameter budgets. These differences are reflected in model geometry. Weight-space profiles expose how each parameterization interacts with pretrained spectral structure, while activation-space diagnostics tie forgetting to non-isometric distortion of general-evaluation representations. Raw movement is therefore an insufficient proxy: OFT shifts representations while preserving their relational geometry, whereas PiSSA and full finetuning induce stronger distortion. Interpolation, used as a pathwise diagnostic, further shows that final SFT checkpoints can drift past a better target-retention operating point, and that interpolation paths should respect each method’s update geometry. PEFT methods should thus be designed not only for target ability acquired, but for the pretrained geometry preserved.

Limitations

This work studies PEFT methods through the stability-plasticity trade-off, and its scope suggests several directions for future work. PEFT-Arena focuses on two reasoning-oriented target domains, mathematics and medicine, and evaluates retention mainly with English general-evaluation suites. Broader multilingual, dialogue, and safety-oriented evaluations would further extend the benchmark.

Our method coverage emphasizes weight-parameterized PEFT methods such as LoRA variants, OFT, IA³, and related baselines. Prompt-, prefix-, and adapter-based methods are also important PEFT families, but their adaptation mechanisms are less directly expressed as explicit weight perturbations. Extending the same evaluation and analogous activation-space diagnostics to these families would make the benchmark more comprehensive.

The internal analyses are empirical diagnostics rather than a complete causal theory of forgetting. They are strongest for characterizing retention-side representation changes, while target-domain plasticity, especially for reasoning-heavy tasks, may require additional task-aligned diagnostics. Similarly, interpolation is used as a pathwise diagnostic and post-hoc trade-off control, with SFT providing the clearest target-retention curves and longer RLVR providing complementary high-*k* evidence.

References

- Armen Aghajanyan, Luke Zettlemoyer, and Sonal Gupta. 2021. Intrinsic dimensionality explains the effectiveness of language model fine-tuning. *ACL*.
- Rahaf Aljundi, Min Lin, Baptiste Goujaud, and Yoshua Bengio. 2019. Gradient based sample selection for online continual learning. *NeurIPS*.
- Alan Ansell, Edoardo Ponti, Anna Korhonen, and Ivan Vulić. 2022. Composable sparse fine-tuning for cross-lingual transfer. In *ACL*.
- Dan Biderman, Jacob Portes, Jose Javier Gonzalez Ortiz, Mansheej Paul, Philip Greengard, Connor Jennings, Daniel King, Sam Havens, Vitaliy Chiley, Jonathan Frankle, and 1 others. 2024. Lora learns less and forgets less. *Transactions on Machine Learning Research*.
- Lucas Caccia, Rahaf Aljundi, Nader Asadi, Tinne Tuytelaars, Joelle Pineau, and Eugene Belilovsky. 2022. New insights on reducing abrupt representation change in online continual learning. In *ICLR*.
- Hanjie Chen, Zhouxiang Fang, Yash Singla, and Mark Dredze. 2025. Benchmarking large language models on answering and explaining challenging medical questions. In *NAACL*.
- Jiaao Chen, Aston Zhang, Xingjian Shi, Mu Li, Alex Smola, and Diyi Yang. 2023. Parameter-efficient fine-tuning design spaces. In *ICLR*.
- Shoufa Chen, Chongjian Ge, Zhan Tong, Jiangliu Wang, Yibing Song, Jue Wang, and Ping Luo. 2022. Adapterformer: Adapting vision transformers for scalable visual recognition. In *NeurIPS*.
- Yupeng Chen, Senmiao Wang, Yushun Zhang, Zhihang Lin, Haozhe Zhang, Weijian Sun, Tian Ding, and Ruoyu Sun. 2024. Mofo: Momentum-filtered optimizer for mitigating forgetting in llm fine-tuning. *arXiv preprint arXiv:2407.20999*.
- MohammadReza Davari, Nader Asadi, Sudhir Mudur, Rahaf Aljundi, and Eugene Belilovsky. 2022. Probing representation forgetting in supervised and unsupervised continual learning. In *CVPR*.
- Muxi Diao, Lele Yang, Wuxuan Gong, Yutong Zhang, Zhonghao Yan, Yufei Han, Kongming Liang, Weiran Xu, and Zhanyu Ma. 2026. Entropy-adaptive fine-tuning: Resolving confident conflicts to mitigate forgetting. *arXiv preprint arXiv:2601.02151*.
- Frances Ding, Jean-Stanislas Denain, and Jacob Steinhardt. 2021. Grounding representation similarity through statistical testing. *NeurIPS*.
- Abhimanyu Dubey, Abhinav Jauhri, Abhinav Pandey, Abhishek Kadian, Ahmad Al-Dahle, Aiesha Letman, Akhil Mathur, Alan Schelten, Amy Yang, Angela Fan, and others. 2024. The llama 3 herd of models. *arXiv preprint arXiv:2407.21783*.
- Ali Edalati, Marzieh Tahaei, Ivan Kobyzev, Vahid Partovi Nia, James J Clark, and Mehdi Rezagholizadeh. 2022. Krona: Parameter efficient tuning with kronecker adapter. *arXiv preprint arXiv:2212.10650*.
- Mozhdeh Gheini, Xiang Ren, and Jonathan May. 2021. Cross-attention is all you need: Adapting pretrained transformers for machine translation. In *EMNLP*.
- Demi Guo, Alexander M Rush, and Yoon Kim. 2021. Parameter-efficient transfer learning with diff pruning. *ACL*.
- Junxian He, Chunting Zhou, Xueze Ma, Taylor Berg-Kirkpatrick, and Graham Neubig. 2021. Towards a unified view of parameter-efficient transfer learning. *ICLR*.
- Neil Houlsby, Andrei Giurgiu, Stanislaw Jastrzebski, Bruna Morrone, Quentin De Laroussilhe, Andrea Gesmundo, Mona Attariyan, and Sylvain Gelly. 2019. Parameter-efficient transfer learning for nlp. In *ICML*.

- Edward J Hu, Yelong Shen, Phillip Wallis, Zeyuan Allen-Zhu, Yuanzhi Li, Shean Wang, Lu Wang, and Weizhu Chen. 2022. LoRA: Low-rank adaptation of large language models. In *ICLR*.
- Xiaoke Huang, Juncheng Wu, Hui Liu, Xianfeng Tang, and Yuyin Zhou. 2025. m1: Unleash the potential of test-time scaling for medical reasoning in large language models. In *Machine Learning for Health*.
- Hugging Face. 2025. Open R1: a fully open reproduction of DeepSeek-R1.
- Gabriel Ilharco, Marco Tulio Ribeiro, Mitchell Wortsman, Ludwig Schmidt, Hannaneh Hajishirzi, and Ali Farhadi. 2023. Editing models with task arithmetic. In *ICLR*.
- Menglin Jia, Luming Tang, Bor-Chun Chen, Claire Cardie, Serge Belongie, Bharath Hariharan, and Ser-Nam Lim. 2022. Visual prompt tuning. In *ECCV*.
- Shibo Jie and Zhi-Hong Deng. 2023. Fact: Factor-tuning for lightweight adaptation on vision transformer. In *AAAI*.
- Di Jin, Eileen Pan, Nassim Oufattole, Wei-Hung Weng, Hanyi Fang, and Peter Szolovits. 2021. What disease does this patient have? A large-scale open domain question answering dataset from medical exams. *Applied Sciences*.
- Qiao Jin, Bhuwan Dhingra, Zhengping Liu, William Cohen, and Xinghua Lu. 2019. PubMedQA: a dataset for biomedical research question answering. In *EMNLP*.
- Jiale Kang and Qingyu Yin. 2026. Miss: Revisiting the trade-off in lora with an efficient shard-sharing structure. *ICLR*.
- Rabeeh Karimi Mahabadi, James Henderson, and Sebastian Ruder. 2021. Compacter: Efficient low-rank hypercomplex adapter layers. In *NeurIPS*.
- James Kirkpatrick, Razvan Pascanu, Neil Rabinowitz, Joel Veness, Guillaume Desjardins, Andrei A Rusu, Kieran Milan, John Quan, Tiago Ramalho, Agnieszka Grabska-Barwinska, and 1 others. 2017. Overcoming catastrophic forgetting in neural networks. *PNAS*.
- Anat Kleiman, Gintare Karolina Dziugaite, Jonathan Frankle, Sham Kakade, and Mansheej Paul. 2025. Soup to go: mitigating forgetting during continual learning with model averaging. *arXiv preprint arXiv:2501.05559*.
- Dawid Jan Kopiczko, Tijmen Blankevoort, and Yuki M Asano. 2024. VeRA: Vector-based random matrix adaptation. In *ICLR*.
- Simon Kornblith, Mohammad Norouzi, Honglak Lee, and Geoffrey Hinton. 2019. Similarity of neural network representations revisited. In *ICML*.
- Tom Kwiatkowski, Jennimaria Palomaki, Olivia Redfield, Michael Collins, Ankur Parikh, Chris Alberti, Danielle Epstein, Illia Polosukhin, Jacob Devlin, Kenton Lee, Kristina Toutanova, Llion Jones, Matthew Kelcey, Ming-Wei Chang, Andrew M. Dai, Jakob Uszkoreit, Quoc Le, and Slav Petrov. 2019. Natural Questions: A Benchmark for Question Answering Research. *TACL*.
- Brian Lester, Rami Al-Rfou, and Noah Constant. 2021. The power of scale for parameter-efficient prompt tuning. *EMNLP*.
- Xiang Lisa Li and Percy Liang. 2021. Prefix-tuning: Optimizing continuous prompts for generation. In *ACL*.
- Dongze Lian, Daquan Zhou, Jiashi Feng, and Xinchao Wang. 2022. Scaling & shifting your features: A new baseline for efficient model tuning. In *NeurIPS*.
- Yan-Shuo Liang and Wu-Jun Li. 2024. Inflora: Interference-free low-rank adaptation for continual learning. In *CVPR*.
- Hunter Lightman, Vineet Kosaraju, Yura Burda, Harri Edwards, Bowen Baker, Teddy Lee, Jan Leike, John Schulman, Ilya Sutskever, and Karl Cobbe. 2023. Let’s verify step by step. *arXiv preprint arXiv:2305.20050*.
- Jiacheng Lin, Zhongruo Wang, Kun Qian, Tian Wang, Arvind Srinivasan, Hansi Zeng, Ruo Chen Jiao, Xie Zhou, Jiri Gesi, Dakuo Wang, and 1 others. 2025. Sft doesn’t always hurt general capabilities: Revisiting domain-specific fine-tuning in llms. *arXiv preprint arXiv:2509.20758*.
- Yong Lin, Hangyu Lin, Wei Xiong, Shizhe Diao, Jianmeng Liu, Jipeng Zhang, Rui Pan, Haoxiang Wang, Wenbin Hu, Hanning Zhang, and 1 others. 2024. Mitigating the alignment tax of rlhf. In *EMNLP*.
- Haokun Liu, Derek Tam, Mohammed Muqeeth, Jay Mohata, Tenghao Huang, Mohit Bansal, and Colin Raffel. 2022a. Few-shot parameter-efficient fine-tuning is better and cheaper than in-context learning. In *NeurIPS*.
- Shih-Yang Liu, Chien-Yi Wang, Hongxu Yin, Pavlo Molchanov, Yu-Chiang Frank Wang, Kwang-Ting Cheng, and Min-Hung Chen. 2024a. DoRA: Weight-decomposed low-rank adaptation. *arXiv preprint arXiv:2402.09353*.
- Weiyang Liu, Rongmei Lin, Zhen Liu, James M Rehg, Liam Paull, Li Xiong, Le Song, and Adrian Weller. 2021. Orthogonal over-parameterized training. In *CVPR*.
- Weiyang Liu, Zeju Qiu, Yao Feng, Yuliang Xiu, Yuxuan Xue, Longhui Yu, Haiwen Feng, Zhen Liu, Juyeon Heo, Songyou Peng, Yandong Wen, Michael J. Black, Adrian Weller, and Bernhard Schölkopf. 2024b. Parameter-efficient orthogonal finetuning via butterfly factorization. In *ICLR*.

- Xiao Liu, Kaixuan Ji, Yicheng Fu, Weng Tam, Zhengxiao Du, Zhilin Yang, and Jie Tang. 2022b. P-tuning: Prompt tuning can be comparable to fine-tuning across scales and tasks. In *ACL*.
- Ekdeep Singh Lubana, Puja Trivedi, Danai Koutra, and Robert Dick. 2022. How do quadratic regularizers prevent catastrophic forgetting: The role of interpolation. In *Conference on Lifelong Learning Agents*, pages 819–837. PMLR.
- Gen Luo, Minglang Huang, Yiyi Zhou, Xiaoshuai Sun, Guannan Jiang, Zhiyu Wang, and Rongrong Ji. 2023. Towards efficient visual adaptation via structural reparameterization. *arXiv preprint arXiv:2302.08106*.
- Mao-Lin Luo, Zi-Hao Zhou, Yi-Lin Zhang, Yuanyu Wan, Tong Wei, and Min-Ling Zhang. 2026. KeepLora: Continual learning with residual gradient adaptation. *arXiv preprint arXiv:2601.19659*.
- Yuning Mao, Lambert Mathias, Rui Hou, Amjad Almahairi, Hao Ma, Jiawei Han, Wen-tau Yih, and Madian Khabsa. 2022. Unipelt: A unified framework for parameter-efficient language model tuning. *ACL*.
- Charles H Martin and Michael W Mahoney. 2021. Implicit self-regularization in deep neural networks: Evidence from random matrix theory and implications for learning. *JMLR*.
- Michael S Matena and Colin A Raffel. 2022. Merging models with fisher-weighted averaging. In *NeurIPS*.
- Fanxu Meng, Zhaohui Wang, and Muhan Zhang. 2024. PiSSA: Principal Singular Values and Singular Vectors Adaptation of Large Language Models. *NeurIPS*.
- Martial Mermillod, Aurélie Bugaiska, and Patrick Bonin. 2013. The stability-plasticity dilemma: Investigating the continuum from catastrophic forgetting to age-limited learning effects. *Frontiers in psychology*, 4:504.
- Ari Morcos, Maithra Raghu, and Samy Bengio. 2018. Insights on representational similarity in neural networks with canonical correlation. *NeurIPS*.
- Sagnik Mukherjee, Lifan Yuan, Dilek Hakkani-Tur, and Hao Peng. 2025. Reinforcement learning finetunes small subnetworks in large language models. *arXiv preprint arXiv:2505.11711*.
- Ankit Pal, Logesh Kumar Umapathi, and Malaikanan Sankarasubbu. 2022. MedMCQA: a large-scale multi-subject multi-choice dataset for medical domain question answering. In *Proceedings of the conference on health, inference, and learning*, PMLR.
- Ashwinee Panda, Berivan Isik, Xiangyu Qi, Sanmi Koyejo, Tsachy Weissman, and Prateek Mittal. 2024. Lottery ticket adaptation: Mitigating destructive interference in llms. *arXiv preprint arXiv:2406.16797*.
- Zeju Qiu, Weiyang Liu, Haiwen Feng, Yuxuan Xue, Yao Feng, Zhen Liu, Dan Zhang, Adrian Weller, and Bernhard Schölkopf. 2023. Controlling text-to-image diffusion by orthogonal finetuning. In *NeurIPS*.
- Zeju Qiu, Weiyang Liu, Adrian Weller, and Bernhard Schölkopf. 2025. Orthogonal finetuning made scalable. In *EMNLP*.
- Maithra Raghu, Justin Gilmer, Jason Yosinski, and Jascha Sohl-Dickstein. 2017. Svcca: Singular vector canonical correlation analysis for deep learning dynamics and interpretability. *NeurIPS*.
- Vinay Venkatesh Ramasesh, Ethan Dyer, and Maithra Raghu. 2021. Anatomy of catastrophic forgetting: Hidden representations and task semantics. In *ICLR*.
- David Rein, Betty Li Hou, Asa Cooper Stickland, Jackson Petty, Richard Yuanzhe Pang, Julien Dirani, Julian Michael, and Samuel R. Bowman. 2024. GPQA: a graduate-level google-proof Q&a benchmark. In *COLM*.
- Sunny Sanyal, Hayden Prairie, Rudrajit Das, Ali Kavis, and Sujay Sanghavi. 2025. Upweighting easy samples in fine-tuning mitigates forgetting. *arXiv preprint arXiv:2502.02797*.
- Zhihong Shao, Peiyi Wang, Qihao Zhu, Runxin Xu, Junxiao Song, Xiao Bi, Haowei Zhang, Mingchuan Zhang, YK Li, Yang Wu, and 1 others. 2024. Deepseekmath: Pushing the limits of mathematical reasoning in open language models. *arXiv preprint arXiv:2402.03300*.
- Kexuan Shi, Yandong Wen, and Weiyang Liu. 2025. Model merging with functional dual anchors. *arXiv preprint arXiv:2510.21223*.
- Daniel L Silver and Robert E Mercer. 2002. The task rehearsal method of life-long learning: Overcoming impoverished data. In *Conference of the Canadian Society for Computational Studies of Intelligence*, pages 90–101. Springer.
- Yi-Lin Sung, Jaemin Cho, and Mohit Bansal. 2022. Lst: Ladder side-tuning for parameter and memory efficient transfer learning. In *NeurIPS*.
- Yi-Lin Sung, Varun Nair, and Colin A Raffel. 2021. Training neural networks with fixed sparse masks. *NeurIPS*.
- Mirac Suzgun, Nathan Scales, Nathanael Schärli, Sebastian Gehrmann, Yi Tay, Hyung Won Chung, Aakanksha Chowdhery, Quoc V Le, Ed H Chi, Denny Zhou, , and Jason Wei. 2023. Challenging BIG-bench tasks and whether chain-of-thought can solve them. *ACL Findings*.
- Rishabh Tiwari, Krishnateja Killamsetty, Rishabh Iyer, and Pradeep Shenoy. 2022. Gcr: Gradient coreset based replay buffer selection for continual learning. In *CVPR*.

- Tu Vu, Brian Lester, Noah Constant, Rami Al-Rfou, and Daniel Cer. 2022. Spot: Better frozen model adaptation through soft prompt transfer. In *ACL*.
- Hanqing Wang, Yixia Li, Shuo Wang, Guanhua Chen, and Yun Chen. 2025. Milora: Harnessing minor singular components for parameter-efficient llm fine-tuning. In *NAACL*.
- Liyuan Wang, Xingxing Zhang, Hang Su, and Jun Zhu. 2024a. A comprehensive survey of continual learning: Theory, method and application. *TPAMI*.
- Xiao Wang, Tianze Chen, Qiming Ge, Han Xia, Rong Bao, Rui Zheng, Qi Zhang, Tao Gui, and Xuan-Jing Huang. 2023. Orthogonal subspace learning for language model continual learning. In *EMNLP Findings*.
- Yaqing Wang, Subhabrata Mukherjee, Xiaodong Liu, Jing Gao, Ahmed Hassan Awadallah, and Jianfeng Gao. 2022. Adamix: Mixture-of-adapter for parameter-efficient tuning of large language models. In *EMNLP*.
- Yubo Wang, Xueguang Ma, Ge Zhang, Yuansheng Ni, Abhranil Chandra, Shiguang Guo, Weiming Ren, Aaran Arulraj, Xuan He, Ziyang Jiang, Tianle Li, Max Ku, Kai Wang, Alex Zhuang, Rongqi Fan, Xiang Yue, and Wenhui Chen. 2024b. MMLU-pro: a more robust and challenging multi-task language understanding benchmark. In *NeurIPS*.
- Mitchell Wortsman, Gabriel Ilharco, Jong Wook Kim, Mike Li, Simon Kornblith, Rebecca Roelofs, Raphael Gontijo Lopes, Hannaneh Hajishirzi, Ali Farhadi, Hongseok Namkoong, and 1 others. 2022. Robust fine-tuning of zero-shot models. In *CVPR*.
- Prateek Yadav, Derek Tam, Leshem Choshen, Colin Raffel, and Mohit Bansal. 2023. TIES-merging: Resolving interference when merging models. In *NeurIPS*.
- A Yang, Baosong Yang, B Zhang, B Hui, B Zheng, B Yu, Chengpeng Li, D Liu, F Huang, H Wei, and others. 2024. Qwen2.5 technical report. *arXiv preprint*.
- Sihan Yang, Kexuan Shi, and Weiyang Liu. 2026. Orthogonal model merging. *arXiv preprint arXiv:2602.05943*.
- Elad Ben Zaken, Yoav Goldberg, and Shauli Ravfogel. 2022. BitFit: Simple Parameter-efficient Fine-tuning for Transformer-based Masked Language-models. In *ACL*.
- Qingru Zhang, Minshuo Chen, Alexander Bukharin, Pengcheng He, Yu Cheng, Weizhu Chen, and Tuo Zhao. 2023. Adalora: Adaptive budget allocation for parameter-efficient fine-tuning. In *ICLR*.
- Yuanhan Zhang, Kaiyang Zhou, and Ziwei Liu. 2024. Neural prompt search. *TPAMI*.
- Jeffrey Zhou, Tianjian Lu, Swaroop Mishra, Siddhartha Brahma, Sujoy Basu, Yi Luan, Denny Zhou, and Le Hou. 2023. Instruction-following evaluation for large language models. *arXiv preprint arXiv:2311.07911*.
- Hanqing Zhu, Zhenyu Zhang, Hanxian Huang, DiJia Su, Zechun Liu, Jiawei Zhao, Igor Fedorov, Hamed Pirsiavash, Zhizhou Sha, Jinwon Lee, and 1 others. 2025. The path not taken: R1vr provably learns off the principals. *arXiv preprint arXiv:2511.08567*.
- Yuxin Zuo, Shang Qu, Yifei Li, Zhang-Ren Chen, Xuekai Zhu, Ermo Hua, Kaiyan Zhang, Ning Ding, and Bowen Zhou. 2025. MedxpertQA: Benchmarking expert-level medical reasoning and understanding. In *ICML*.

Appendix

Table of Contents

A	Related Work	14
B	Implementation and Evaluation Details	16
B.1	Model and Training Details	16
B.2	Evaluation Protocol	16
B.3	Artifacts, Licenses, and Reproducibility	16
C	Expanded Benchmark Results	16
C.1	Expanded General-Capability Benchmarks	16
C.2	Expanded Task-Level Scores for the Main Benchmark	18
D	Additional Weight-Space Geometry Results	21
D.1	Full Spectral Profiles and Retention Smoothness	21
D.2	OFT Singular-Vector Alignment	21
D.3	Capability-Conditioned Drift	22
E	Additional Activation-Space Geometry Results	24
E.1	Metric Definitions	24
E.2	Coverage and Experimental Setup	24
E.3	Layer/Module Method-Family Summaries	24
F	Interpolation and Rewinding Follow-ups	25
F.1	Interpolation Setup	25
F.2	Full SFT Interpolation Curves	26
F.3	OFT Linear vs Cayley Path	26
F.4	Layer-wise Rewinding Results	27
F.5	Additive PEFT Rewinding Variants	28
F.6	Longer-RLVR High-k Interpolation	28

A Related Work

PEFT methods. Parameter-efficient finetuning (PEFT) specializes large pretrained models by optimizing only a small subset of parameters, substantially reducing computational overhead while often achieving performance comparable to full finetuning (Houlsby et al., 2019; Aghajanyan et al., 2021; Hu et al., 2022; Edalati et al., 2022; Wang et al., 2022; Gheini et al., 2021; Zaken et al., 2022; Guo et al., 2021; Sung et al., 2021; Ansell et al., 2022; Lester et al., 2021; Li and Liang, 2021; Vu et al., 2022; He et al., 2021; Mao et al., 2022; Karimi Mahabadi et al., 2021; Liu et al., 2022a; Sung et al., 2022; Chen et al., 2023; Jia et al., 2022; Chen et al., 2022; Zhang et al., 2024; Jie and Deng, 2023; Lian et al., 2022; Luo et al., 2023). Prior PEFT methods can be broadly grouped into three categories. (1) *Additive weight reparameterization.* A representative approach is Low-Rank Adaptation (LoRA) (Hu et al., 2022), which freezes pretrained weights and introduces a learnable low-rank update to enable efficient task adaptation with a small number of trainable parameters. Subsequent work extends LoRA along several complementary dimensions. Methods such as AdaLoRA (Zhang et al., 2023) focus on adaptive rank allocation by dynamically re-allocating rank budgets during training, and DoRA (Liu et al., 2024a) improves optimization by decoupling update magnitude from direction. Other approaches modify the update structure: MISS (Kang and Yin, 2026) replaces the two-factor decomposition with a single expanded low-rank matrix, and VeRA (Kopiczko et al., 2024) attains high effective update rank through shared, frozen random projection matrices modulated by lightweight trainable scaling vectors. Another line of work explores initialization strategies informed by the spectral properties of pretrained weights. PiSSA (Meng et al., 2024) initializes low-rank factors using principal singular components, whereas MiLoRA (Wang et al., 2025) instead targets minor components by initializing updates on the minor singular subspace while freezing the principal components. (2) *Constrained weight updates.* Beyond low-rank additive updates, Orthogonal Finetuning (OFT) (Qiu et al., 2023; Liu et al., 2024b; Qiu et al., 2025) constrains the learned transformations to be orthogonal. By preserving the spectral properties of the original weight matrices, such constraints act as an implicit regularizer during adaptation and provide an alternative form of structured parameter efficiency. (3) *Activation- and prompt-based adaptation.* Instead of directly modifying weight matrices, this line of work introduces auxiliary parameters to modulate intermediate representations. For instance, IA³ learns per-channel scaling vectors that element-wise modulate key activations (Liu et al., 2022a). Similarly, Prompt Tuning (Liu et al., 2022b) and Prefix-Tuning (Li and Liang, 2021) prepend trainable continuous embeddings to the input layer or to hidden states across attention blocks, respectively. These methods facilitate task specialization by re-contextualizing frozen representations, effectively inducing localized shifts in the activation space.

Continual learning. Continual learning (CL) aims to incorporate new knowledge while preserving previously acquired capabilities, thereby mitigating catastrophic forgetting (Wang et al., 2024a). Prior CL approaches are commonly categorized into data-replay-based methods (Aljundi et al., 2019; Silver and Mercer, 2002; Tiwari et al., 2022), which require access to historical training data, and data-free methods (Wortsman et al., 2022; Lubana et al., 2022; Chen et al., 2024; Panda et al., 2024), which avoid replay by relying instead on architectural constraints or regularization. These data-free CL methods are relevant to our setting because they aim to preserve prior capabilities without replaying the original pretraining data. This paradigm operates directly in parameter space, bypassing the need for historical data. Standard approaches employ ℓ_2 regularization (Kirpatrick et al., 2017) or model merging (Wortsman et al., 2022; Lubana et al., 2022; Kleiman et al., 2025; Lin et al., 2024) to anchor finetuned parameters to the base model, thereby balancing stability and plasticity. For PEFT, O-LoRA (Wang et al., 2023) and InfLoRA (Liang and Li, 2024) enforce orthogonality between sequential task-specific subspaces to mitigate forgetting. However, these methods are designed mainly for sequential continual-learning protocols, whereas PEFT-Arena studies one-shot post-training and evaluates retention of pretrained capabilities after a single adaptation run. KeepLoRA (Luo et al., 2026) constrains updates to the non-principal subspace of the original weights, protecting the principal components that encode general capabilities.

Catastrophic forgetting in LLMs. While traditional CL primarily addresses multi-task sequential learning, recent focus has shifted toward catastrophic forgetting during the post-training of LLMs,

particularly when finetuning on distributions that diverge significantly from the pre-training data (Sanyal et al., 2025; Lin et al., 2025). A prevailing hypothesis identifies the discrepancy between on-policy and off-policy distributions as a primary driver of forgetting. To bridge this gap, several data-centric strategies aim to simulate on-policy learning via reweighting. FLOW (Sanyal et al., 2025) prioritizes simpler samples to stabilize updates, while TALR (Lin et al., 2025) and EAFT (Diao et al., 2026) mitigate forgetting by attenuating learning rates or weights for tokens with high difficulty or low information entropy. These methods are complementary to our study, focusing at the data, loss, or optimizer level, while PEFT-Arena focuses on comparing PEFT parameterizations and analyzing how their parameter-space and activation-space geometry lead to different stability-plasticity trade-offs. Despite the effectiveness of these data-level interventions, a fundamental question remains: how do these stability-promoting effects manifest in the model’s underlying parameter space? Emerging evidence in reinforcement learning suggests that optimization stability is intrinsically linked to parameter-space dynamics. Recent studies also suggest that retention can be linked to parameter-space dynamics, such as preferentially updating non-principal weight components (Zhu et al., 2025; Mukherjee et al., 2025), and that LoRA may retain pretrained knowledge better than full finetuning (Biderman et al., 2024). PEFT-Arena builds on these observations by evaluating multiple PEFT families under a unified protocol and by connecting external trade-offs to internal geometry diagnostics.

Model averaging and interpolation. Task arithmetic (Ilharco et al., 2023) shows that meaningful task-specific knowledge is encoded in weight differences $W_{\text{ft}} - W_{\text{pre}}$, and that scaling or combining these “task vectors” enables modular control over model behavior. Model soups (Wortsman et al., 2022) average checkpoints for improved robustness. WiSE-FT (Wortsman et al., 2022) interpolates between zero-shot and finetuned weights to improve robustness under distribution shift while maintaining target performance. TIES merging (Yadav et al., 2023) resolves sign conflicts across task vectors. Fisher merging (Matena and Raffel, 2022) uses second-order information for weighted combinations. Orthogonal merging (Yang et al., 2026) combines task-specific weights on orthogonal manifolds. Functional dual anchors (Shi et al., 2025) merge task vectors within input-representation space. These methods primarily combine multiple task-specialized models. Our use of interpolation is related in form but different in purpose. Rather than proposing a new model-merging technique, merging multiple task-specialized models, or targeting distribution-shift robustness, we use interpolation as a pathwise diagnostic for single-task PEFT. By sweeping the interpolation coefficient α between the base and finetuned model, we trace explicit stability-plasticity trade-off curves and diagnose when final SFT checkpoints overshoot a better target-retention operating point. We further emphasize that the interpolation path should respect the natural coordinates of each PEFT parameterization.

Spectral analysis of neural networks. The singular value spectrum of weight matrices has long been recognized as informative about network behavior. Heavy-tail spectral theory connects weight matrix spectra to generalization (Martin and Mahoney, 2021), and recent work in reinforcement learning has linked stability to preferential updating of non-principal weight components (Zhu et al., 2025; Mukherjee et al., 2025). (Biderman et al., 2024) empirically observes that LoRA retains pretrained knowledge better than full finetuning, but the spectral mechanisms underlying this observation remain unexplored. (Liu et al., 2021; Qiu et al., 2023) explicitly link the pretrained knowledge retention to spectrum preservation. Our spectral analysis specifically targets PEFT updates, decomposing changes into retention and adaptation profiles and using them as descriptive diagnostics of update geometry. These weight-space diagnostics are complemented by activation-space analysis, which measures whether finetuning preserves representations on general-evaluation data. This offers a systematic spectral framework that connects internal geometric properties of PEFT updates to external stability-plasticity outcomes.

Representation similarity and activation geometry. Neural representation similarity has been widely studied using CCA-based metrics, SVCCA, PWCCA, and CKA (Kornblith et al., 2019; Raghu et al., 2017; Morcos et al., 2018). CKA compares centered Gram matrices and is now a standard diagnostic for representation similarity (Kornblith et al., 2019), while recent benchmarking studies show that orthogonal Procrustes is a strong and interpretable baseline for comparing neural representations (Ding et al., 2021).

This perspective is also relevant to forgetting: prior work studies catastrophic forgetting through hidden representation changes and shows that forgetting can manifest as representation drift, often in deeper

layers (Ramasesh et al., 2021; Davari et al., 2022). Continual-learning studies further argue that reducing representation drift on previously learned data can mitigate forgetting (Caccia et al., 2022). Motivated by these works, we analyze PEFT-induced changes in general-capability activations. In particular, we distinguish raw movement from non-isometric distortion: orthogonal transformations preserve inner products, distances, and angles, so large activation movement is not necessarily destructive. We therefore use Procrustes residual, pairwise Gram distortion, and CKA to measure whether finetuning preserves the relational geometry of pretrained representations.

B Implementation and Evaluation Details

B.1 Model and Training Details

Compute. All experiments are conducted on $8 \times$ NVIDIA H100 80GB GPUs, each by a single run. The total compute varies by model, method, and training regime; for instance, a typical LoRA SFT run (Math / Medical training, target and general evaluation) takes approximately 100 GPU-hours for 7B models and 60 GPU-hours for 3B models. A 200-step RLVR runs require approximately 200 GPU-hours. Diagnostic analyses are run offline and do not require additional model training.

SFT. We use an effective batch size of 256, a maximum response length of 8192 tokens, and train for 4 epochs. Full fine-tuning uses a learning rate of 5×10^{-5} , while all PEFT methods use 2×10^{-4} . We adopt a cosine decay learning-rate scheduler.

RL. We use a rollout batch size of 256, a mini-batch size of 64 for gradient accumulation, and a group size of 8. The maximum generation length is set to 8192 tokens, consistent with SFT and evaluation. Full fine-tuning uses a learning rate of 10^{-6} , while all PEFT methods use 10^{-5} . Unless otherwise specified, RL experiments are trained for 200 steps. For the longer-training study in subsection 2.2, we additionally train to 500 steps.

B.2 Evaluation Protocol

We elaborate the evaluation settings for tasks of different domains below.

Math. Each math problem is evaluated by average accuracy@16, with a maximum response length of 8192 tokens (consistent with training) and temperature $T = 0.6$.

Medical. We use average accuracy as the primary metric with temperature $T = 0.0$.

General. We follow the evaluation configuration in OpenCompass¹ with context length 1024, temperature $T = 0.0$, and one sample per query.

B.3 Artifacts, Licenses, and Reproducibility

We use publicly available model checkpoints, PEFT implementations, evaluation datasets, and benchmark frameworks, and cite their creators in the main text and related work. We use these artifacts under their respective licenses and usage terms. The evaluated models, trainable parameter counts, PEFT configurations, training hyperparameters, decoding settings, context length, and evaluation protocol are described in this appendix. We provide code and configurations at <https://github.com/Sphere-AI-Lab/PEFT-Arena> to support reproducibility, subject to the licenses and terms of the underlying artifacts. We do not collect new user data or human-subject data. For public benchmark datasets, we rely on their original curation and use them only for controlled research evaluation.

C Expanded Benchmark Results

C.1 Expanded General-Capability Benchmarks

To test whether the original General axis transfers beyond IFEval/NQ/BBH, we further evaluate representative checkpoints on HumanEval, HellaSwag, WinoGrande, MMLU(avg), ARC, and GSM8K. The expanded benchmarks are used as consistency checks for the General axis rather than as a separate main benchmark suite. The detailed per-task scores are reported in Table 6.

¹<https://github.com/open-compass/opencompass>

Method	HumanE.	Hella.	Wino.	MMLU	ARC	GSM8K	Avg.
A: Llama, RL-Math							
Full FT	58.54	64.40	56.99	62.38	76.95	79.15	66.40
OFT-b32	59.76	64.75	53.91	62.07	75.59	78.47	65.76
LoRA-r8	59.76	64.17	55.72	62.25	77.63	77.71	66.21
B: Llama, SFT-Math							
Full FT	54.88	63.77	12.71	59.83	41.69	71.80	50.78
OFT-b16	55.49	60.97	22.89	59.78	65.76	75.82	56.79
OFT-b128	54.88	60.05	15.47	57.99	50.17	70.28	51.47
LoRA-r4	54.88	63.18	11.60	56.82	41.02	72.48	50.00
LoRA-r8	48.78	63.54	12.23	58.41	39.66	73.54	49.36
LoRA-r16	35.98	60.09	12.31	58.37	40.34	71.34	46.41
LoRA-r32	40.85	60.71	14.84	58.87	39.32	69.98	47.43
AdaLoRA-r8	54.88	62.30	13.34	58.66	41.02	62.32	48.75
PiSSA-r8	0.00	24.79	4.89	25.18	12.54	1.97	11.56
MiSS-r8	49.39	57.06	24.63	57.76	47.46	69.75	51.01
MiSS-r64	39.02	53.67	23.91	55.65	41.36	69.90	47.25
VeRA-r256	56.10	62.08	57.54	62.24	71.86	77.48	64.55
DoRA-r8	39.63	63.03	13.26	57.97	39.32	71.65	47.48
IA ³	54.27	57.74	54.85	61.45	69.49	76.19	62.33
C: Llama, SFT-Med							
Full FT	48.78	57.33	17.13	58.76	40.34	72.71	49.18
OFT-b16	51.83	61.49	13.89	58.36	60.68	76.35	53.77
OFT-b32	51.83	60.04	15.15	58.13	55.59	74.75	52.58
OFT-b64	45.12	58.98	14.21	59.13	52.20	74.75	50.73
OFT-b128	41.46	56.96	14.52	59.15	41.69	74.22	48.00
LoRA-r4	52.44	58.68	14.52	58.22	45.76	74.15	50.63
LoRA-r8	27.44	59.24	15.63	59.13	49.15	73.62	47.37
LoRA-r16	22.56	57.90	17.68	58.31	39.66	73.77	44.98
AdaLoRA-r8	51.22	59.04	13.26	56.90	46.10	74.98	50.25
MiSS-r8	47.56	60.22	16.10	56.20	44.41	71.27	49.29
MiSS-r64	41.46	53.42	18.47	53.87	32.54	66.34	44.35
DoRA-r8	33.54	59.60	14.84	58.52	49.49	74.60	48.43
IA ³	53.05	60.52	56.83	61.28	65.42	75.13	62.04
D: Qwen, RL-Math							
Full FT	76.83	84.88	61.01	52.89	29.32	83.44	64.73
OFT-b32	74.39	84.97	62.35	59.13	35.09	81.50	66.24
LoRA-r8	76.83	85.15	62.04	61.92	35.93	83.02	67.48
E: Qwen, SFT-Math							
Full FT	71.34	76.59	60.22	29.68	33.90	75.13	57.81
OFT-b16	70.73	82.14	60.54	30.93	37.63	83.32	60.88
OFT-b32	75.00	78.98	59.35	28.88	35.25	82.41	59.98
OFT-b64	75.61	82.27	61.80	29.11	34.58	81.65	60.84
OFT-b128	75.00	73.64	61.40	29.41	29.15	80.67	58.21
LoRA-r4	75.61	69.79	61.64	29.24	33.56	65.73	55.93
AdaLoRA-r8	75.00	64.20	60.54	29.39	34.92	57.24	53.55
PiSSA-r8	0.61	24.89	46.65	23.28	45.42	16.30	26.19
VeRA-r256	74.39	83.67	63.61	50.29	32.88	84.84	64.95
DoRA-r8	76.22	76.63	61.80	29.52	33.56	75.44	58.86
F: Qwen, SFT-Med							
Full FT	77.44	72.91	66.54	28.96	32.54	75.44	58.97
OFT-b32	77.44	70.61	65.59	28.67	32.88	85.06	60.04
OFT-b64	78.05	74.08	65.04	27.86	26.78	85.82	59.61
LoRA-r4	78.05	55.91	64.48	27.47	31.19	84.99	57.02
LoRA-r16	65.24	58.72	63.69	27.55	34.24	85.75	55.87
LoRA-r32	65.24	62.70	60.85	27.32	33.90	85.97	56.00
MiLoRA-r8	78.05	59.62	64.01	27.41	31.86	82.79	57.29
MiSS-r8	65.24	61.31	61.40	28.50	25.42	79.83	53.62
MiSS-r64	72.56	60.94	56.27	32.03	39.32	77.71	56.47
PiSSA-r8	17.68	24.91	45.94	9.54	50.17	39.58	31.30
VeRA-r256	71.95	83.37	61.17	57.85	33.90	80.59	64.81

Table 6: Expanded general-capability raw results on additional benchmarks. We report HumanEval, HellaSwag, WinoGrande, MMLU(avg), ARC, and GSM8K for the same settings used in the main benchmark. For duplicated raw rows in Qwen2.5-7B RL-math (Full FT / OFT-b32), values are consolidated by averaging non-null duplicate entries after dropping missing values. “-” denotes unavailable evaluations.

C.2 Expanded Task-Level Scores for the Main Benchmark

For completeness, we expand each average score in [Table 1](#) into its constituent task-level accuracies. Math target averages are computed over Math-500, AIME24, and AMC23 ([Table 7](#)). Medical target averages are computed over the eleven medical benchmarks used in the main benchmark ([Table 8](#)). General averages are computed over IFEval (Inst-level-strict-accuracy), NQ, and the BBH average ([Table 9](#)).

Config	Qwen2.5-7B-base				Llama3.2-3B-Instruct			
	Math-500	AIME24	AMC23	Avg.	Math-500	AIME24	AMC23	Avg.
SFT/Base	61.30	7.10	37.50	35.30	49.20	9.80	24.40	27.80
SFT/Full FT	79.10	17.50	55.30	50.63	56.40	10.80	34.50	33.90
SFT/OFT-b16	71.30	11.20	44.50	42.33	52.30	6.00	30.00	29.43
SFT/OFT-b32	75.00	14.20	51.60	46.93	53.30	6.20	32.30	30.60
SFT/OFT-b64	74.70	14.60	49.40	46.23	53.30	6.00	28.60	29.30
SFT/OFT-b128	76.70	15.80	50.80	47.77	55.40	5.40	35.90	32.23
SFT/LoRA-r4a8	70.60	9.80	46.60	42.33	43.50	3.80	25.60	24.30
SFT/LoRA-r8a16	71.20	10.00	46.20	42.47	45.40	3.50	23.30	24.07
SFT/LoRA-r16a32	72.70	13.50	48.40	44.87	46.90	2.50	25.50	24.97
SFT/LoRA-r32a64	74.10	12.50	49.50	45.37	49.50	1.50	26.70	25.90
SFT/AdaLoRA-r8a16	68.50	10.00	42.80	40.43	41.40	0.60	20.50	20.83
SFT/PiSSA-r8a16	72.30	12.10	49.20	44.53	1.50	0.00	0.50	0.67
SFT/MiLoRA-r8a16	70.50	11.50	45.80	42.60	43.60	2.50	24.70	23.60
SFT/KeepLoRA-r8	68.00	9.80	43.80	40.53	30.30	2.30	13.00	15.20
SFT/MiSS-r8	71.00	12.10	46.40	43.17	44.00	0.80	25.30	23.37
SFT/MiSS-r64	75.90	13.80	51.10	46.93	52.10	2.70	31.10	28.63
SFT/VeRA-r256	67.70	7.50	43.10	39.43	51.60	9.20	25.60	28.80
SFT/DoRA-r8a16	71.80	10.20	45.00	42.33	44.50	1.50	25.50	23.83
SFT/IA3	61.80	5.80	37.80	35.13	52.20	6.90	30.00	29.70
RLVR/Full FT	76.10	13.90	52.70	47.57	52.80	10.40	26.20	29.80
RLVR/OFT-b32	74.40	16.50	52.80	47.90	51.00	10.00	28.90	29.97
RLVR/LoRA-r8a16	74.80	11.40	54.60	46.93	51.80	8.30	26.40	28.83

Table 7: Detailed math target scores for the checkpoints in [Table 1](#).

Config	GPQA	HLE	Lancet	MMLU-Pro	MB-op4	MB-op5	MedMCQA	MedQA	MedXpert	NEJM	PubMedQA	Avg.
SFT/Qwen/Base	48.72	17.09	57.28	53.42	47.40	39.94	51.49	58.13	12.15	54.89	69.40	46.36
SFT/Llama/Base	37.69	15.82	50.97	44.17	38.96	34.09	46.69	51.92	14.08	47.76	73.70	41.44
SFT/Qwen/Full FT	47.44	12.66	61.65	64.43	59.09	57.79	60.79	70.46	16.77	62.52	76.30	53.63
SFT/Llama/Full FT	36.92	10.76	53.64	45.41	49.03	45.13	51.45	59.54	14.01	52.24	68.70	44.26
SFT/Qwen/OFT-b16	37.69	13.29	54.37	54.98	52.27	39.94	54.20	60.17	12.97	55.72	72.30	46.17
SFT/Llama/OFT-b16	31.03	13.29	46.60	39.54	44.16	35.39	46.98	52.08	13.11	46.10	63.10	39.22
SFT/Qwen/OFT-b32	42.56	13.92	57.77	57.98	51.62	46.10	55.20	63.47	15.04	57.71	73.50	48.63
SFT/Llama/OFT-b32	31.79	10.13	47.09	39.41	44.16	37.01	46.40	52.47	12.15	46.43	67.50	39.50
SFT/Qwen/OFT-b64	40.51	8.86	59.71	61.11	55.52	46.43	56.06	67.01	16.22	59.20	73.50	49.47
SFT/Llama/OFT-b64	31.03	9.49	45.63	41.30	46.75	38.64	47.50	54.99	12.56	50.25	67.20	40.77
SFT/Qwen/OFT-b128	41.54	17.09	61.89	63.39	59.42	53.57	58.95	67.79	15.80	61.03	73.60	52.40
SFT/Llama/OFT-b128	35.38	8.86	48.79	43.13	45.45	43.18	49.18	56.17	12.42	49.92	68.20	42.17
SFT/Qwen/LoRA-r4a8	37.18	13.92	59.95	57.00	48.70	44.16	53.62	62.84	14.15	55.56	71.20	47.12
SFT/Llama/LoRA-r4a8	27.18	12.03	42.23	38.44	37.99	37.66	44.01	50.43	11.94	41.63	62.60	36.92
SFT/Qwen/LoRA-r8a16	42.56	14.56	57.77	57.26	50.32	46.75	54.58	62.22	13.87	55.39	71.70	47.91
SFT/Llama/LoRA-r8a16	29.74	12.03	46.12	40.52	39.61	34.74	45.49	51.61	12.77	42.62	66.50	38.34
SFT/Qwen/LoRA-r16a32	38.21	10.76	55.10	61.11	52.60	44.81	54.08	63.86	14.35	59.70	71.90	47.86
SFT/Llama/LoRA-r16a32	33.85	15.19	44.90	38.76	42.21	39.61	44.23	49.18	12.97	44.28	66.10	39.21
SFT/Qwen/LoRA-r32a64	40.77	11.39	55.34	60.52	58.77	47.08	55.25	64.89	16.70	59.54	74.00	49.48
SFT/Llama/LoRA-r32a64	25.38	12.66	50.24	38.96	45.78	37.99	46.12	50.04	11.94	48.09	65.40	39.33
SFT/Qwen/AdaLoRA-r8a16	37.95	13.92	54.37	54.40	44.81	41.88	52.47	60.96	14.29	54.23	68.20	45.22
SFT/Llama/AdaLoRA-r8a16	34.36	10.13	41.75	37.98	43.18	34.09	44.85	48.86	10.21	41.96	60.80	37.11
SFT/Qwen/PiSSA-r8a16	29.23	17.09	28.88	22.21	27.27	21.43	34.21	30.56	10.01	24.05	46.10	26.16
SFT/Llama/PiSSA-r8a16	20.00	16.46	25.24	16.03	25.32	19.81	26.03	25.53	10.56	21.89	26.00	21.17
SFT/Qwen/MiLoRA-r8a16	42.82	9.49	56.31	58.63	49.03	40.26	52.76	62.53	14.08	59.04	70.20	46.83
SFT/Llama/MiLoRA-r8a16	27.18	13.92	45.39	37.52	38.64	36.04	44.47	50.04	11.73	41.46	67.60	37.64
SFT/Qwen/KeepLoRA-r8	42.05	12.03	57.04	53.55	44.48	39.61	51.40	60.33	13.60	55.22	72.30	45.60
SFT/Llama/KeepLoRA-r8	37.18	18.99	48.06	39.67	44.16	40.58	47.33	54.52	11.80	43.62	67.90	41.26
SFT/Qwen/MiSS-r8	35.90	14.56	61.89	59.61	49.35	47.40	56.61	65.51	16.29	58.04	71.10	48.75
SFT/Llama/MiSS-r8	32.31	16.46	47.09	40.26	43.51	39.61	45.71	50.98	10.84	47.93	67.10	40.16
SFT/Qwen/MiSS-r64	45.90	12.66	58.74	62.08	57.79	53.25	58.69	67.95	17.12	61.19	75.50	51.90
SFT/Llama/MiSS-r64	39.49	9.49	46.60	39.80	44.81	45.78	50.18	54.99	13.39	48.59	68.40	41.96
SFT/Qwen/VeRA-r256	34.10	15.19	38.83	34.40	24.03	19.81	35.38	30.95	11.66	38.47	30.70	28.50
SFT/Llama/VeRA-r256	34.36	14.56	48.79	45.08	41.56	35.71	47.38	50.51	12.15	46.93	70.50	40.68
SFT/Qwen/DoRA-r8a16	38.46	14.56	58.01	56.87	56.49	43.18	53.45	64.96	13.25	58.54	70.70	48.04
SFT/Llama/DoRA-r8a16	26.67	14.56	43.20	38.63	40.91	38.96	45.16	49.02	11.87	44.61	67.20	38.25
SFT/Qwen/IA3	26.41	11.39	37.62	24.36	30.52	27.92	36.60	35.82	11.25	31.67	57.30	30.08
SFT/Llama/IA3	42.05	18.99	48.79	40.91	42.53	34.74	46.59	52.40	12.63	45.94	44.90	39.13
RLVR/Qwen/Full FT	39.23	13.92	53.40	58.63	48.38	45.45	52.00	58.05	15.32	50.08	73.50	46.24
RLVR/Llama/Full FT	42.31	14.56	50.73	50.23	48.70	45.45	53.93	58.60	13.18	51.74	75.20	45.88
RLVR/Qwen/OFT-b32	41.28	17.72	56.55	56.81	47.40	43.51	52.43	61.04	14.15	52.24	71.60	46.79
RLVR/Llama/OFT-b32	38.46	15.19	53.16	49.90	45.78	40.91	51.11	59.47	13.32	53.23	74.40	44.99
RLVR/Qwen/LoRA-r8a16	50.00	14.56	53.88	59.09	46.75	34.42	54.55	61.27	15.11	56.05	72.20	47.08
RLVR/Llama/LoRA-r8a16	47.69	12.66	50.97	46.78	48.38	45.13	50.44	60.33	13.53	49.92	68.90	44.97

Table 8: Detailed medical target scores for the checkpoints in Table 1.

Config	Adapt.	Qwen2.5-7B-base				Llama3.2-3B-Instruct			
		IFEval	NQ	BBH	Avg.	IFEval	NQ	BBH	Avg.
SFT/Base	Math	45.32	26.40	69.18	46.97	77.58	31.75	49.75	53.03
SFT/Base	Med	45.32	26.40	69.18	46.97	79.26	31.75	59.28	56.76
SFT/Full FT	Math	36.69	2.13	63.85	34.22	66.79	30.17	22.52	39.83
SFT/Full FT	Med	36.33	0.86	66.04	34.41	46.40	12.80	18.88	26.03
SFT/OFT-b16	Math	41.25	18.17	68.34	42.58	67.75	26.59	28.91	41.08
SFT/OFT-b16	Med	41.25	25.43	68.58	45.09	69.78	29.00	24.12	40.97
SFT/OFT-b32	Math	41.13	24.74	67.10	44.37	66.67	26.32	29.19	40.73
SFT/OFT-b32	Med	40.53	18.01	68.65	42.40	69.30	28.48	23.72	40.50
SFT/OFT-b64	Math	38.97	2.80	66.15	35.97	66.55	26.76	25.93	39.75
SFT/OFT-b64	Med	38.61	9.64	69.08	39.11	65.23	28.45	19.43	37.70
SFT/OFT-b128	Math	37.53	7.81	65.58	36.98	63.31	24.90	20.57	36.26
SFT/OFT-b128	Med	37.77	3.60	69.28	36.88	56.47	27.31	18.98	34.26
SFT/LoRA-r4a8	Math	38.13	19.39	67.47	41.66	58.39	27.15	21.84	35.79
SFT/LoRA-r4a8	Med	35.13	6.40	67.73	36.42	52.76	21.63	21.13	31.84
SFT/LoRA-r8a16	Math	34.53	16.70	66.43	39.22	63.07	26.62	20.02	36.57
SFT/LoRA-r8a16	Med	35.01	5.90	68.57	36.06	48.32	16.59	19.06	27.99
SFT/LoRA-r16a32	Math	34.41	3.80	66.52	34.91	61.63	27.65	23.37	37.55
SFT/LoRA-r16a32	Med	33.33	3.68	67.55	34.86	48.44	20.03	19.06	29.18
SFT/LoRA-r32a64	Math	35.01	13.80	65.81	38.21	62.35	26.79	22.46	37.20
SFT/LoRA-r32a64	Med	35.25	3.68	67.57	35.50	50.12	20.80	21.14	30.69
SFT/AdaLoRA-r8a16	Math	32.61	6.65	66.98	35.41	56.35	25.79	21.45	34.53
SFT/AdaLoRA-r8a16	Med	32.97	11.16	67.88	37.34	60.43	26.98	21.46	36.29
SFT/PiSSA-r8a16	Math	33.57	6.87	33.88	24.78	24.70	1.52	3.01	9.74
SFT/PiSSA-r8a16	Med	30.10	4.24	19.82	18.05	19.18	3.85	15.73	12.92
SFT/MiLoRA-r8a16	Math	37.65	7.59	67.62	37.62	61.99	25.62	19.14	35.59
SFT/MiLoRA-r8a16	Med	34.17	5.24	68.22	35.88	48.32	18.75	20.61	29.23
SFT/KeepLoRA-r8	Math	41.73	20.30	69.22	43.75	68.11	27.56	26.54	40.74
SFT/KeepLoRA-r8	Med	45.32	26.68	69.27	47.09	67.63	28.98	21.95	39.52
SFT/MiSS-r8	Math	39.45	14.60	63.30	39.12	58.75	20.36	22.68	33.93
SFT/MiSS-r8	Med	36.45	3.96	62.87	34.43	49.04	23.60	22.48	31.71
SFT/MiSS-r64	Math	35.85	2.74	59.72	32.77	60.91	20.69	23.28	34.96
SFT/MiSS-r64	Med	35.37	0.69	62.08	32.72	39.81	8.37	20.17	22.78
SFT/VeRA-r256	Math	46.04	27.12	68.59	47.25	72.66	31.80	34.85	46.79
SFT/VeRA-r256	Med	45.92	25.79	69.31	47.01	72.18	31.66	42.98	48.94
SFT/DoRA-r8a16	Math	36.81	17.56	66.36	40.25	60.55	26.70	19.70	35.65
SFT/DoRA-r8a16	Med	34.05	6.54	67.58	36.06	47.00	17.87	17.73	27.53
SFT/IA3	Math	43.17	23.49	67.46	44.71	70.14	29.53	37.49	45.72
SFT/IA3	Med	48.44	27.15	69.16	48.25	72.30	29.97	34.73	45.67
RLVR/Full FT	Math	50.00	25.84	70.20	48.68	76.50	31.02	49.08	52.20
RLVR/Full FT	Med	42.69	17.45	69.51	43.22	76.98	31.02	47.44	51.81
RLVR/OFT-b32	Math	49.64	27.51	69.55	48.90	74.94	28.50	46.68	50.04
RLVR/OFT-b32	Med	46.40	26.48	68.84	47.24	76.50	30.58	49.85	52.31
RLVR/LoRA-r8a16	Math	48.44	26.95	69.40	48.27	77.10	31.36	48.06	52.17
RLVR/LoRA-r8a16	Med	48.44	11.08	68.88	42.80	76.98	31.72	51.91	53.53

Table 9: Detailed general-benchmark scores for the checkpoints in Table 1.

D Additional Weight-Space Geometry Results

D.1 Full Spectral Profiles and Retention Smoothness

To complement the qualitative fluctuation description in [section 3](#), we quantify how the retention-side fluctuation score correlates with actual retention performance across the main-results checkpoints. For a profile $s(i)$ and its local moving average $\bar{s}(i)$, we define

$$\text{Fluc}(s) = \frac{1}{n} \sum_{i=1}^n |s(i) - \bar{s}(i)|. \quad (6)$$

The retention-side fluctuation score is the mean absolute deviation of the diagonal-projection retention spectrum from this local moving average; larger values indicate a spikier, less smooth retention profile. In our implementation, we use a moving-average window of size $w = 5$ (equivalently, radius $r = 2$), apply reflect padding at the two boundaries before computing the 1D moving average, and set the score to zero when the spectrum length is shorter than the window. [Table 10](#) shows that larger retention fluctuation is significantly associated with lower general performance and more forgetting. The correlation is computed on the full set of matched checkpoints and the SFT subset. Additional visualization of weight-space profiles in [Figure 5](#) shows that different PEFT parameterizations perturb the pretrained spectrum in qualitatively different ways. Full finetuning and PiSSA produce the most visible retention-side disruption, while OFT keeps a more coherent diagonal-projection profile. LoRA, MiSS, PiSSA, and AdaLoRA all show uneven update-energy allocation, matching the large adaptation-side fluctuation scores shown in the main-text fluctuation-score bar plot in [Figure 2](#). PiSSA is especially distinctive: its update is strongest on the principal components, but it also remains spiky and non-negligible across the remaining ranks rather than being confined to only the top singular directions. In contrast, OFT’s profile is more structured under its orthogonal parameterization, and the RL variants generally show smaller and more coherent perturbations than their SFT counterparts.

Subset	n	General score		Forgetting	
		Spearman ρ	p -value	Spearman ρ	p -value
All checkpoints	88	-0.622	9.3×10^{-10}	0.557	9.8×10^{-8}
SFT only	76	-0.413	5.2×10^{-4}	0.329	6.6×10^{-3}

Table 10: Spearman correlation between retention-side fluctuation and retention metrics. Larger fluctuation is associated with lower retained general ability and more forgetting.

D.2 OFT Singular-Vector Alignment

OFT requires a parameterization-aware interpretation because its effective update is an orthogonal transformation rather than a generic additive perturbation. The main text therefore focuses on diagnostics that can be compared across PEFT families: retention/adaptation profiles, capability-conditioned drift, and activation-geometry distortion. For completeness, we include an OFT-specific singular-vector alignment (SVA) diagnostic here to isolate the rotational component of OFT.

Let $W_0 = U_0 \Sigma_0 V_0^\top$. Under an ideal right-multiplicative OFT rotation,

$$W^* = W_0 R = U_0 \Sigma_0 V_0^\top R, \quad R^\top R = I.$$

The singular values are preserved, while the right singular vectors rotate. We therefore compare the cosine similarity between corresponding pretrained and rotated singular vectors to measure how strongly OFT changes singular-vector orientation. As shown in [Figure 6](#), RL-trained OFT exhibits a relatively uniform rotation pattern across components, consistent with a more global and coherent transformation of the layer weight. In contrast, SFT-trained OFT shows localized SVA spikes in specific layers and components, indicating that some singular directions receive disproportionately large rotations. This explains why OFT can mitigate forgetting through its orthogonal constraint while still showing residual retention loss under SFT: the update preserves singular values, but non-uniform rotations can still perturb directions used by general capabilities.

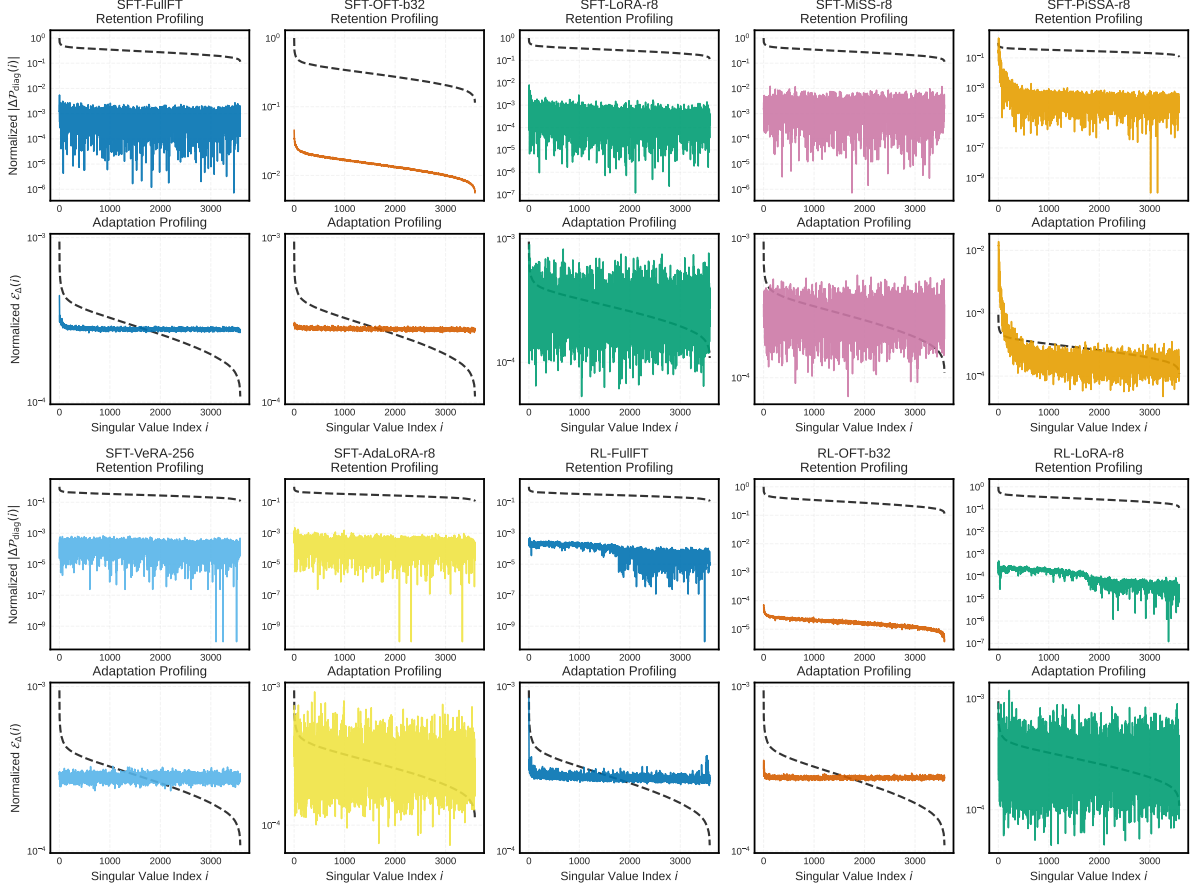


Figure 5: Additional weight-space profiles for SFT. We visualize diagonal-projection changes on the pretrained singular basis (retention profile) and projected update energy over pretrained directions (adaptation profile).

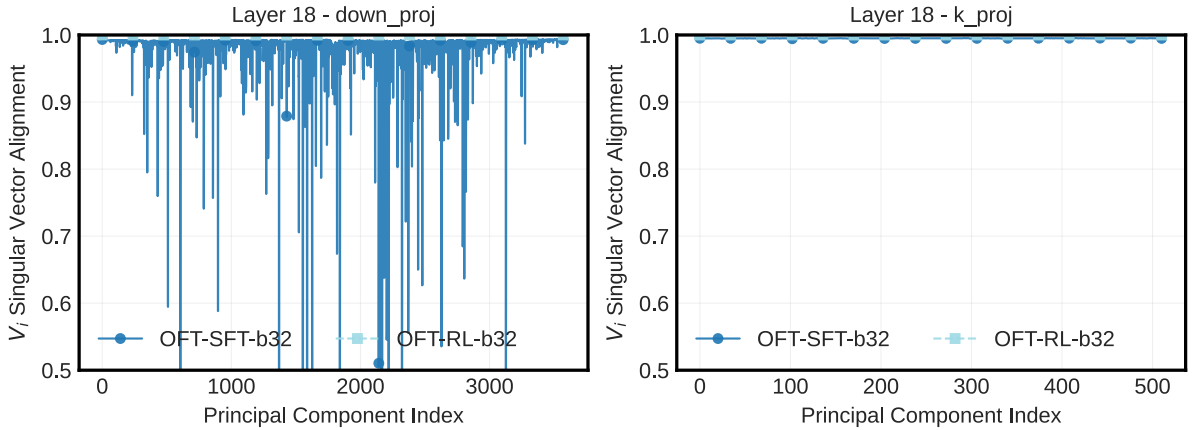


Figure 6: Additional OFT geometry diagnostic using singular vector alignment (SVA). OFT primarily changes singular-vector orientation while preserving singular values.

D.3 Capability-Conditioned Drift

The retention and adaptation profiles in subsection 3.1 describe an update in the pretrained singular basis, but they are not conditioned on which directions are actually used by a capability distribution. Capability-conditioned spectral drift (CSD) adds this data dependence. For a selected module, we collect the pretrained-model input activations h on a dataset D , then measure the output displacement induced by

the effective weight update $\Delta W = W^* - W_0$.

In our implementation, the selected module is layer 18 mlp. `down_proj.weight`. For each checkpoint, W^* is the effective finetuned weight: full-finetuned checkpoints are read directly, while PEFT adapters are merged into the base weight before extracting W^* . We use 161 general examples from IFEval/NQ/BBH for D_G , and 165–170 examples from the corresponding math or medical target domain for D_T . Activations are always collected from the pretrained model so that all methods are compared on the same capability-conditioned input distribution. The tables below report the SFT-only subset of the available CSD results.

For a dataset D , absolute CSD is defined as

$$\text{CSD}_{\text{abs}}(D) = \mathbb{E}_{h \sim D} [\|\Delta W h\|_2^2].$$

This quantity is a capability-conditioned projection of the update profile: if $h = \sum_i a_i v_i$ in the pretrained right singular basis, then $\Delta W h = \sum_i a_i \Delta W v_i$. Thus, directions that are both strongly updated and frequently activated by D contribute more to CSD. We also report a relative version that controls for the scale of the pretrained module output,

$$\text{CSD}_{\text{rel}}(D) = \frac{\mathbb{E}_{h \sim D} [\|\Delta W h\|_2^2]}{\mathbb{E}_{h \sim D} [\|W_0 h\|_2^2] + \epsilon},$$

and an update-normalized version that partially controls for raw update magnitude,

$$\text{CSD}_{\text{un}}(D) = \frac{\mathbb{E}_{h \sim D} [\|\Delta W h\|_2^2]}{(\|\Delta W\|_F^2 + \epsilon)(\mathbb{E}_{h \sim D} [\|h\|_2^2] + \epsilon)}.$$

We compute these quantities for the general distribution D_G and the target distribution D_T , and summarize both CSD_G and the general-to-target ratio $\text{CSD}_G / (\text{CSD}_T + \epsilon)$. The ratio is intended to describe whether a given update perturbs general-capability activations disproportionately relative to target-domain activations. As with the spectral profiles, CSD is an empirical diagnostic rather than a causal proof.

Metric	External metric	Pearson	Spearman
$\text{CSD}_{G,\text{rel}}$	Forgetting	0.347	0.317
$\text{CSD}_{G,\text{un}}$	Forgetting	0.481	0.603
$\text{CSD}_{T,\text{rel}}$	Target gain	-0.164	0.107
$\text{CSD}_{T,\text{un}}$	Target gain	-0.358	-0.615
$\text{Ratio}_{\text{rel}}$	Forgetting	-0.188	-0.241

Table 11: CSD correlations over the SFT-only subset ($n = 68$ checkpoints) at layer18 mlp. `down_proj.weight`. General CSD is positively associated with forgetting, while target CSD does not provide a monotonic explanation of target gain.

Family	n	$\text{CSD}_{G,\text{rel}}$	$\text{CSD}_{T,\text{rel}}$	Ratio	Forget
Full FT	4	1.16×10^{-3}	1.06×10^{-3}	1.077	17.31
LoRA	16	1.21×10^{-3}	1.21×10^{-3}	1.042	15.70
OFT	16	7.82×10^{-3}	7.64×10^{-3}	1.018	11.20
PiSSA	4	8.94×10^{-2}	8.37×10^{-2}	1.102	34.56
MiLoRA	4	7.17×10^{-4}	6.46×10^{-4}	1.288	16.35
MISS	8	1.93×10^{-2}	1.88×10^{-2}	1.019	18.13

Table 12: Method-family CSD summary on the SFT-only subset. OFT has larger raw relative CSD than LoRA/Full FT because an orthogonal rotation can induce substantial Euclidean output movement, but its general-to-target ratio remains close to one and lower than Full FT, LoRA, PiSSA, and MiLoRA. PiSSA is the clearest outlier in both general CSD and forgetting.

Interpretation. The CSD results complement the weight-space profiles in two ways. First, general-distribution CSD is a useful retention-side diagnostic: $\text{CSD}_{G,\text{rel}}$ is positively correlated with forgetting, and the update-normalized version remains positively correlated in rank order. This is consistent with the view that perturbing directions activated by general-evaluation data is associated with retention loss.

Second, target-distribution CSD should not be used as a proxy for target gain; the correlation with target gain is weak or negative, consistent with the view that reasoning-heavy target improvements depend on task-aligned computation rather than update magnitude alone. Finally, raw CSD must be interpreted with the PEFT parameterization in mind. In particular, OFT can have higher Euclidean drift because orthogonal rotations move vectors, motivating the activation-geometry diagnostics used in the main text.

E Additional Activation-Space Geometry Results

E.1 Metric Definitions

The main text focuses on Procrustes residual, CKA, and pairwise Gram distortion. Secondary diagnostics such as raw residual, angular drift, norm drift, and Procrustes improvement are used as controls to separate pointwise movement from non-isometric representation distortion.

For centered activations X_0 and X_1 , Procrustes residual is

$$d_{\text{proc}} = \frac{\min_{R^T R=I} \|X_1 R - X_0\|_F}{\|X_0\|_F + \epsilon}.$$

Linear CKA is computed from centered activations:

$$\text{CKA}(X_0, X_1) = \frac{\|X_0^T X_1\|_F^2}{\|X_0^T X_0\|_F \|X_1^T X_1\|_F + \epsilon}.$$

For row-normalized token activations Z_0 and Z_1 , pairwise Gram distortion is

$$d_{\text{gram}} = \frac{\|Z_1 Z_1^T - Z_0 Z_0^T\|_F}{\|Z_0 Z_0^T\|_F + \epsilon}.$$

E.2 Coverage and Experimental Setup

We run the activation-geometry analysis on the SFT subset of the main-table checkpoints for Qwen2.5-7B and Llama3.2-3B-Instruct. For each checkpoint, we compare base and finetuned full-forward module outputs on general data (IFEval/NQ/BBH) and the corresponding target-domain data. We use eight module locations: layer 9 and layer 18, each with q_proj, k_proj, v_proj, and mlp.down_proj. In total, the compiled tables use 20 SFT checkpoints and 160 general-distribution rows for the correlation analysis.

E.3 Layer/Module Method-Family Summaries

Layer	Module	Full FT	LoRA	OFT	MiLoRA	PiSSA
		Forgetting=17.31 Proc. / Gram / CKA	Forgetting=15.97 Proc. / Gram / CKA	Forgetting=7.81 Proc. / Gram / CKA	Forgetting=16.35 Proc. / Gram / CKA	Forgetting=34.56 Proc. / Gram / CKA
9	self_attn.q_proj	0.169 / 0.029 / 0.965	0.174 / 0.025 / 0.965	0.114 / 0.014 / 0.985	0.172 / 0.024 / 0.965	0.625 / 0.137 / 0.524
9	self_attn.k_proj	0.182 / 0.040 / 0.971	0.182 / 0.037 / 0.974	0.118 / 0.027 / 0.990	0.175 / 0.036 / 0.978	0.665 / 0.217 / 0.609
9	self_attn.v_proj	0.195 / 0.195 / 0.931	0.203 / 0.235 / 0.921	0.138 / 0.141 / 0.966	0.202 / 0.239 / 0.926	0.649 / 1.370 / 0.369
9	mlp.down_proj	0.117 / 0.211 / 0.898	0.121 / 0.219 / 0.902	0.074 / 0.151 / 0.964	0.117 / 0.219 / 0.915	0.452 / 1.598 / 0.518
18	self_attn.q_proj	0.190 / 0.016 / 0.951	0.195 / 0.016 / 0.955	0.145 / 0.011 / 0.980	0.190 / 0.016 / 0.960	0.521 / 0.066 / 0.627
18	self_attn.k_proj	0.201 / 0.049 / 0.966	0.205 / 0.042 / 0.970	0.160 / 0.026 / 0.983	0.204 / 0.037 / 0.974	0.570 / 0.169 / 0.697
18	self_attn.v_proj	0.211 / 0.212 / 0.913	0.223 / 0.239 / 0.909	0.172 / 0.169 / 0.951	0.211 / 0.246 / 0.923	0.536 / 0.752 / 0.522
18	mlp.down_proj	0.164 / 0.250 / 0.865	0.181 / 0.243 / 0.856	0.128 / 0.191 / 0.934	0.164 / 0.248 / 0.865	0.438 / 0.865 / 0.440

Table 13: Activation-geometry method-family averages on general-evaluation data across tested layer/module locations for SFT checkpoints. Each cell reports Proc./Gram/CKA; lower Proc. and Gram and higher CKA indicate better geometry preservation. Column headers report method-family forgetting.

The full results of activation geometry method-family averages are shown in Table 13. These metrics are primarily retention-side diagnostics. They do not show a simple monotonic relationship with target-domain gain, likely because reasoning-heavy target improvements depend on task-aligned computation and answer margins rather than representation movement magnitude alone.

F Interpolation and Rewinding Follow-ups

F.1 Interpolation Setup

This appendix provides implementation details and additional results for the interpolation analyses in [section 4](#).

Additive-update PEFT (e.g., LoRA, AdaLoRA, MiSS). For PEFT methods with an additive parameterization,

$$W^* = W_0 + \Delta W, \quad W(\alpha) = W_0 + \alpha \Delta W.$$

Interpolation is implemented by scaling the learned update ΔW . For LoRA, $\Delta W = sBA$ (with method-dependent scale s , e.g., $s = \frac{\alpha_{\text{LoRA}}}{r}$). A simple implementation is to scale both factors,

$$\Delta W(\alpha) = s(\sqrt{\alpha}B)(\sqrt{\alpha}A) = \alpha sBA,$$

which preserves the product structure and avoids excessively scaling a single factor.

OFT: interpolating rotation by scaling the generator. Using the Cayley parameterization, the rotation is hence parameterized by

$$R(Q) = (I + Q)(I - Q)^{-1},$$

where Q is the skew-symmetric generator. We interpolate OFT by scaling its generator,

$$\begin{aligned} R(\alpha) &\triangleq R(\sqrt{\alpha}Q), \\ R(\sqrt{\alpha}Q) &= (I + \sqrt{\alpha}Q)(I - \sqrt{\alpha}Q)^{-1}. \end{aligned}$$

Here α denotes the coefficient applied to rotation strength rather than directly to the generator norm. For small angles, the rotation angle θ satisfies $\|Q\| \approx \tan(\theta/2) \approx \theta/2$, hence θ is approximately linear in $\|Q\|$. Following prior geometric diagnostics, we define the layer-wise rotation strength

$$\rho_\ell \triangleq 1 - \cos(\theta_\ell).$$

Using $\cos \theta \approx 1 - \theta^2/2$ gives $\rho_\ell \approx \theta_\ell^2/2$, and therefore $\rho_\ell \propto \|Q\|^2$. Consequently, to scale the rotation strength by a factor of α in the small-angle regime, we scale the generator by $\sqrt{\alpha}$: $Q' = \sqrt{\alpha}Q$.

F.2 Full SFT Interpolation Curves

Figure 7 provides the full SFT interpolation curves across PEFT methods and target domains. These curves complement the single-column interpolation summary in the main text.

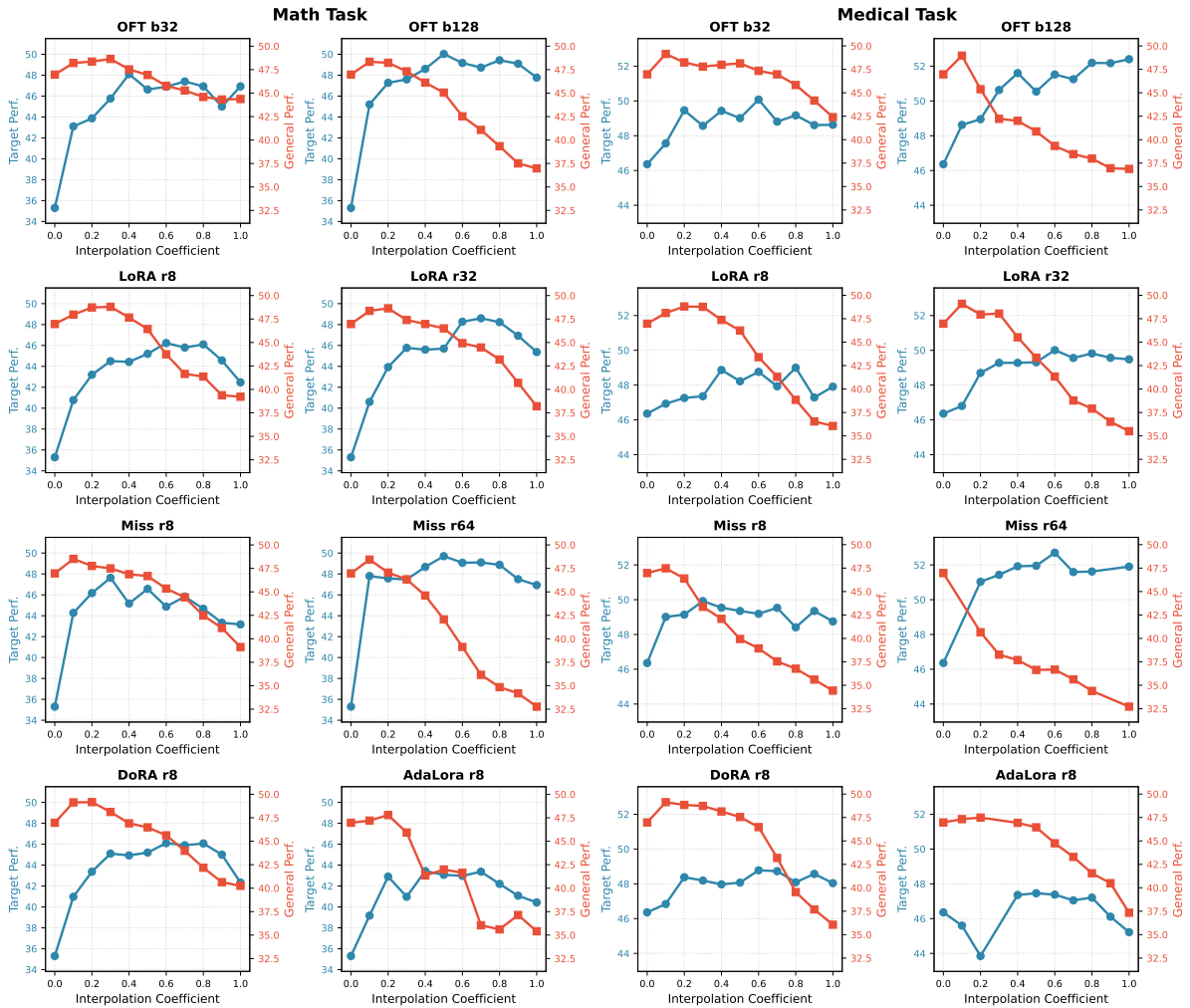


Figure 7: Full SFT interpolation curves across PEFT methods and target domains. These results complement the representative pathwise interpolation analysis in the main text.

F.3 OFT Linear vs Cayley Path

Table 14 reports the full OFT dense-delta versus Cayley-generator interpolation curve referenced in the main text.

Path	α	Math Avg. \uparrow	General \uparrow
Delta interp.	0.1	43.97	43.93
Delta interp.	0.3	43.93	43.91
Delta interp.	0.5	43.93	44.45
Delta interp.	0.7	44.60	43.61
Delta interp.	0.9	44.17	43.97
$\sqrt{\alpha}Q$ interp.	0.1	43.10	48.21
$\sqrt{\alpha}Q$ interp.	0.3	45.77	48.64
$\sqrt{\alpha}Q$ interp.	0.5	46.63	46.93
$\sqrt{\alpha}Q$ interp.	0.7	47.40	45.28
$\sqrt{\alpha}Q$ interp.	0.9	45.00	44.32
Final OFT	1.0	46.93	44.37

Table 14: OFT interpolation path comparison on Qwen2.5-7B math SFT with OFT-b32. Dense-weight interpolation scales $W^* - W_0$, while the OFT path rescales the Cayley generator as $\sqrt{\alpha}Q$.

F.4 Layer-wise Rewinding Results

In the main text, Table 5 reports the OFT layer-wise rewinding case study. Figure 4 compares actual optimization trajectories with interpolation trajectories, while Figure 9 visualizes these OFT rewinding alternatives.

Figure 8 shows the layer-wise OFT update strength used by SafeScale and MinScale. The strength is computed with the same statistic as the rewinding implementation: the average squared Frobenius norm of OFT generator parameters within each layer. Later layers receive substantially larger generator updates than the early layers, motivating layer-wise rewinding rather than a single global coefficient.

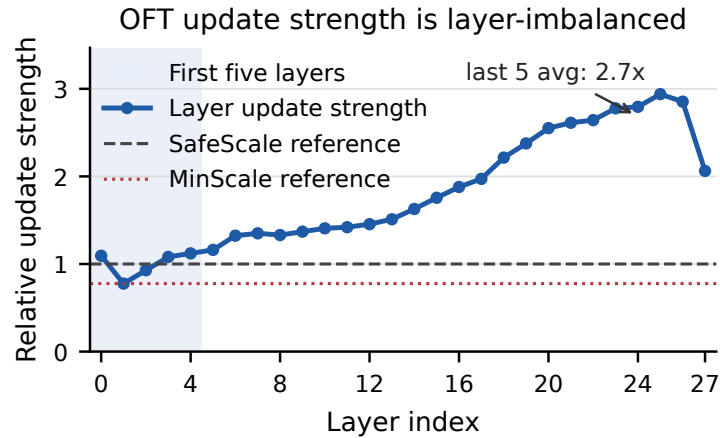


Figure 8: Layer-wise OFT update strength for Qwen2.5-7B math SFT with OFT-b32. Values are normalized by the average strength of the first five layers, which is the SafeScale reference.

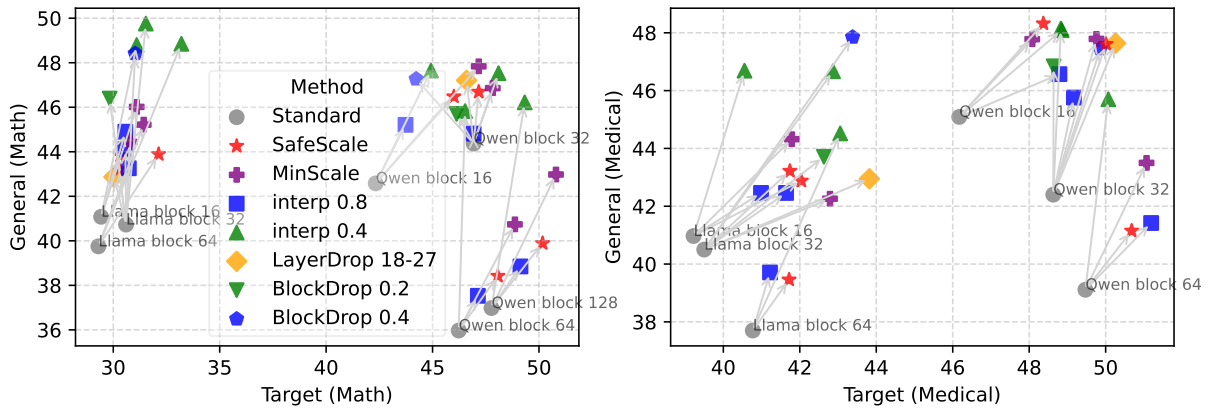


Figure 9: Trade-off alternatives achieve consistent improvement on OFT adapters of different sizes. This figure complements Table 5 by visualizing how different scaling/pruning alternatives behave across adapter sizes.

F.5 Additive PEFT Rewinding Variants

Table 15 shows that beyond OFT, similar layer-wise rewinding variants can also improve additive PEFT methods in this setting.

Method	Variant	Math Avg. \uparrow	General \uparrow
LoRA-r8	Baseline	42.47	39.22
LoRA-r8	SafeScale	43.87	39.55
LoRA-r8	MinScale	44.93	43.11
MiSS-r8	Baseline	43.17	39.12
MiSS-r8	SafeScale	42.60	38.95
MiSS-r8	MinScale	44.83	42.85

Table 15: Additive PEFT rewinding variants on Qwen2.5-7B math SFT. MinScale improves both math and General for LoRA-r8 and MiSS-r8, suggesting that layer-wise rewinding is not limited to OFT.

F.6 Longer-RLVR High-k Interpolation

Table 16 summarizes high- k interpolation follow-ups, where interpolation exposes a clearer overshoot phenomenon than the standard pass@1 view.

Setting	Variant	Pass@64 \uparrow	General \uparrow
OFT-200	Baseline ($\alpha = 1.0$)	77.23	47.58
OFT-200	Best interp. ($\alpha = 0.7$)	78.07	48.39
OFT-200	MinScale	76.13	47.37
OFT-500	Baseline ($\alpha = 1.0$)	75.77	46.93
OFT-500	Best interp. ($\alpha = 0.7$)	78.50	48.04
OFT-500	MinScale	78.47	47.34
LoRA-200	Baseline ($\alpha = 1.0$)	76.73	44.64
LoRA-200	Best interp. ($\alpha = 0.7$)	77.43	47.31
LoRA-500	Baseline ($\alpha = 1.0$)	73.80	43.26
LoRA-500	Best interp. ($\alpha = 0.3$)	75.30	48.05

Table 16: High- k RLVR follow-ups under pass@64. Interpolation can improve both pass@64 and General in several longer-RLVR settings, exposing a pathwise degradation pattern not visible from pass@1 alone.